



HAL
open science

Action-FRET: Probing the molecular conformation of mass-selected gas phase peptides with Förster Resonance Energy Transfer detected by acceptor specific fragmentation

Steven Daly, Frédéric Poussigue, Anne-Laure Simon, Luke Macaleese, Franck Bertorelle, Fabien Chiot, Rodolphe Antoine, Philippe Dugourd

► To cite this version:

Steven Daly, Frédéric Poussigue, Anne-Laure Simon, Luke Macaleese, Franck Bertorelle, et al.. Action-FRET: Probing the molecular conformation of mass-selected gas phase peptides with Förster Resonance Energy Transfer detected by acceptor specific fragmentation. *Analytical Chemistry*, 2014, 86 (17), pp.8798-8804. 10.1021/ac502027y . hal-01344561

HAL Id: hal-01344561

<https://hal.science/hal-01344561>

Submitted on 12 Jul 2016

HAL is a multi-disciplinary open access archive for the deposit and dissemination of scientific research documents, whether they are published or not. The documents may come from teaching and research institutions in France or abroad, or from public or private research centers.

L'archive ouverte pluridisciplinaire **HAL**, est destinée au dépôt et à la diffusion de documents scientifiques de niveau recherche, publiés ou non, émanant des établissements d'enseignement et de recherche français ou étrangers, des laboratoires publics ou privés.

Action-FRET: Probing the molecular conformation of mass-selected gas phase peptides with FRET detected by acceptor specific fragmentation.

Steven Daly,^{a,b} Frédéric Poussigue,^{a,c} Anne-Laure Simon,^{a,b} Luke MacAleese,^{a,b} Franck Bertorelle,^{a,b} Fabien Chirot,^{a,c} Rodolphe Antoine,^{a,b} Philippe Dugourd.^{a,b}

^a Université de Lyon, F-69622, Lyon, France

^b CNRS et Université Lyon 1, UMR5306, Institut Lumière Matière

^c CNRS et Université Lyon 1 UMR 5280, Institut des Sciences Analytiques

Anal. Chem., **2014**, *86* (17), pp 8798–8804

DOI: 10.1021/ac502027y

Action-FRET: Probing the molecular conformation of mass-selected gas phase peptides with FRET detected by acceptor specific fragmentation.

Steven Daly,^{a,b} Frédéric Poussigue,^{a,c} Anne-Laure Simon,^{a,b} Luke MacAleese,^{a,b} Franck Bertorelle,^{a,b} Fabien Chiro,^{a,c} Rodolphe Antoine,^{a,b} Philippe Dugourd.^{a,b}

^a Université de Lyon, F-69622, Lyon, France

^b CNRS et Université Lyon 1, UMR5306, Institut Lumière Matière

^c CNRS et Université Lyon 1 UMR 5280, Institut des Sciences Analytiques

FRET, Mass spectrometry, Ion mobility, gas phase biomolecules, action spectroscopy

ABSTRACT: The use of Förster resonance energy transfer (FRET) as a probe of the structure of biological molecules through fluorescence measurements in solution is well attested. The transposition of this technique to the gas phase is appealing since it opens the perspective of combining the structural accuracy of FRET with the specificity and selectivity of mass spectrometry (MS). Here, we report FRET results on gas phase poly-alanine ions obtained by measuring FRET efficiency through specific photo-fragmentation rather than fluorescence. The structural sensitivity of the method was tested using commercially-available chromophores (QSY 7 and carboxyrhodamine 575) grafted on a series of small, alanine based peptides of differing sizes. The photo-fragmentation of these systems was investigated through action-spectroscopy, and their conformations were probed using ion mobility spectrometry (IMS) and Monte Carlo-minimization (MCM) simulations. We show that specific excitation of the donor chromophore results in the observation of fragments that are specific to the electronic excitation of the acceptor chromophore. This shows that energy transfer took place between the two chromophores and hence that the action-FRET technique can be used as a new and sensitive probe of the structure of gas phase biomolecules, which opens perspectives as a new tool in structural biology.

Introduction

Förster resonance energy transfer (FRET) is a widely used probe of molecular structure in solution.¹⁻⁴ It requires a photon source to electronically excite the so-called ‘donor chromophore’, and a light harvesting setup to detect either the ‘donor’ or ‘acceptor’ chromophore fluorescence. The occurrence of FRET is then usually evidenced through a decrease in the fluorescence of the donor chromophore (quenching), with the concurrent onset of the fluorescence of the acceptor chromophore or by changes in fluorescence decay times. The interpretation of FRET results relies on the known distance dependence of the effect, and on the possibility to graft specific chromophores at relatively well-defined sites on a molecule. FRET is then used to characterize the distance between the chromophores and hence separation between the grafting sites, although extracting exact distances is difficult due to the uncertainty of the exact orientation of the transition dipole moments of the chromophores. This allows the use of FRET to probe intra- or inter-molecular distances, especially the change in distance, depending on whether the

chromophores are attached to the same or to different molecules.

The versatility of FRET makes it a powerful tool to assess the conformation and/or association of molecules. It has been shown that the overall structure of complex molecular edifices can be preserved in the gas-phase using soft ionization techniques.^{5,6} Therefore the development of techniques capable of probing FRET in the gas phase is of high interest, and could be integrated into a global approach for structure determination of proteins and protein complexes.⁷⁻⁹

There are few techniques that allow structural investigation of large systems in vacuo.¹⁰⁻¹² One of the only techniques that can be successfully applied to large molecular edifices is ion mobility spectrometry (IMS), which provides global information on the overall shape of the system.¹³⁻¹⁵ Associated with fluorescence spectroscopy, a few examples of gas-phase FRET have been recorded that very nicely demonstrate the possibility to observe and use FRET in the gas-phase.¹⁶⁻²³

However, fluorescence detectors are difficult to implement efficiently in mass spectrometers and their use has been

limited to a small number of systems. Such ‘out-coupling’ of light is difficult due to restriction of the solid angle of light detection imposed by the geometry of the mass spectrometer. By contrast, ‘in-coupling’ of light – that is the coupling of a mass spectrometer with a light source such as a laser – is simpler and has already been implemented by many groups.²⁴⁻

²⁷ The relative ease of ‘in-coupling’ lends itself to an alternative methodology for monitoring the absorption of photons by ions in a mass spectrometer – namely action spectroscopy. Action spectroscopy monitors the ion photodissociation as a function of the photon energy and this photodissociation is assumed to be correlated to the absorption cross-section of the ion. Action spectroscopy has been widely used to record the photodissociation spectra for a broad range of molecular ions and complexes across a large range of photon energies.²⁸⁻³⁶ Due to the fact that detection of fragment ions is more sensitive than single photon counting methods, such an action spectroscopy methodology for the measurement of FRET will provide a more sensitive probe of molecular structure of gas phase biomolecules, simultaneously with usual MS (including multistage) measurements.

In the following, we show that the high sensitivity of action-spectroscopy can be used as a straightforward tool to detect FRET in the gas phase. A detection scheme will be presented that enables the measurement of FRET by fragment ion detection only.³⁷ Chromophores possessing a large overlap of the fluorescence spectrum of the ‘donor’ with the absorption spectrum of the ‘acceptor’, and with fragmentation of the ‘acceptor’ specific to photo-dissociation were chosen and characterized. Results on a series of alanine based peptides of increasing size demonstrate the feasibility and sensitivity of the action-FRET methodology as a tool for the study of the structure of biomolecules in the gas-phase.

Experimental and theoretical Section

Peptides and Chromophores. The choice of the peptides and chromophores will be discussed in greater detail in the following section. The acceptor chromophore is QSY7 N-succinimidyl ester (Life technologies), a dark quencher absorbing at 560 nm in solution and known to fragment efficiently at 532 nm in the gas phase.³⁸ The donor chromophore is 5-carboxyrhodamine 575 N-succinimidyl ester (rh575) (Life Technologies), absorbing at 550 nm and fluorescing at 575 nm in solution. Rh575 was also used as the donor chromophore by Talbot *et al.*¹⁸ and both the fluorescence excitation and emission spectra along with photo-fragmentation mass spectra have been previously studied in detail.³⁹ Both chromophores are designed to be functionalized onto primary amines, and thus peptides containing two primary amine groups only were chosen. For the initial study, the simple tri-peptide N-alanine-alanine-lysine-OH (AAK) was chosen to ensure that the chromophores remain spatially close to each other in the doubly grafted species. To study the distance dependence of the measured energy transfer, a series of poly-alanine based peptides varying in size from 7 to 19 residues were chosen with a lysine residue at both C- and N-terminus, the N-terminus being capped with an acetyl moiety to meet the condition of only 2 primary amines per molecule. Additionally, to aid the aqueous solubility histidine (H) was inserted at regular intervals along the chain. Thus, the

following three peptides were chosen: KA₂HA₂K, KA₃HA₃K, and KA₅HA₅HA₅K.

The chromophores were grafted both individually and simultaneously onto the peptides. The two chromophores were dissolved in DMSO and the peptides in water, where the concentrations were approximately 10 mM in each case. N-succinimidyl esters are reactive with water, and the hydrolysis is competitive with the amide reaction required for grafting. Thus, it was necessary to use 500 μ l DMSO as the reactive medium for the grafting reactions. For the grafting of either donor or acceptor chromophore to the peptide (resulting in both singly and doubly grafted species) 10 μ l of the chromophore and peptide solutions were added to the reaction medium. For the double grafting reaction with both chromophores, the volumes were adjusted to 14 μ l, 4 μ l and 12 μ l for rh575, QSY7 and peptide solutions respectively, in order to optimize the grafting ratios. The reaction solutions were placed in an oven at 60 °C and left for at least 12 hours, after which the solutions were tested to ensure the reaction was complete. It is important to note that it is possible for each chromophore to graft to the N-terminus or C-terminus primary amine, and thus there will be two doubly grafted species present; (rh575-peptide-QSY7) and (QSY7-peptide-rh575). Examination of the CID mass spectra shows that both species are present in approximately equal amounts (see figure S5). Separation of the two species is not possible; hence all results on the doubly grafted species presented in this work are for this mixture of these two forms. For simplicity we will refer in the text to the doubly grafted species as (rh575-peptide-QSY7). For use in the electrospray ionization source, 20 μ l of the reaction solution was diluted in 3 ml of 1:1 water/methanol with 3 μ l acetic acid.

Mass spectrometry and optical spectroscopy. The experimental setup used to perform the experiments presented in this paper has been described in detail previously.⁴⁰ Briefly, a linear quadrupole ion trap mass spectrometer (LTQ, Thermo Fisher Scientific, San Jose, CA) was used for ion preparation, ion selection and trapping, fragmentation (collision induced dissociation (CID) and photodissociation) and subsequent mass analysis. The back panel of the vacuum manifold was modified by drilling a hole and fitting a quartz window (30 mm diameter and 5 mm thickness). This window was positioned in front of the linear ion trap such as to allow the direct irradiation of trapped ions via a central hole in the trap exit electrode.

The light source used is a Panther EX OPO pumped by the third harmonic (355 nm) of a Surelite II Nd:YAG laser (Continuum, Santa Clara, CA). A repetition rate of 10 Hz and pulse-widths of the order of 5 ns were used. The visible portion of the spectrum was used directly via the signal beam of the OPO (410 – 700 nm), which is collimated and refocused with a long focal distance lens of 500mm. Pulse energies were kept between 0.9 to 1.1 mJ/pulse to avoid saturation. A mechanical shutter, synchronized with the mass spectrometer, is used to stop the beam at all times except the ‘ion activation window’ – that is the time after ion accumulation and before the mass analysis. A single laser pulse was used for the irradiation of the trapped ions. When irradiating ions the normalized collision energy is kept at zero. Laser power is monitored continuously using the reflection portion of the

beam upon passing through an 85:15 beam splitter placed at 45° with respect to the beam. The power is monitored using a power meter (Ophir-Spiricon GmbH, Ahrensburg, Germany). The value of the power used for normalization is taken as the average value over the duration of a measurement, of the order of 5 minutes per wavelength.

Ion mobility mass spectrometry. Ion mobility (IMS) measurements were performed using a custom-built ion mobility spectrometer already described elsewhere.⁴¹ Briefly, a 1 m long drift tube is inserted between an electrospray ionization source and a time-of-flight (ToF) mass spectrometer. Helium at a pressure of 15 Torr is maintained in the drift tube, and the temperature of the whole setup is kept at 300 K. Ions are periodically injected in the drift tube from an hourglass funnel ion trap. Their mass-to-charge ratio and drift time through the tube are simultaneously measured using the ToF. Ion mobilities and collision cross section (CCS) are finally calculated from the evolution of the ion arrival time distribution as a function of the inverse drift voltage.

Monte Carlo simulations. Structures for the doubly grafted peptides were generated using a Monte Carlo minimization (MCM) approach using the Tinker⁴² suite of programs. The choice of force field is constrained by the requirement that the entire system be modelled, and as such the MMFF94 force field⁴³ was chosen as the most suitable to account for all the necessary parameters. Initial geometries were chosen with all peptide dihedral angles in the trans configuration. For the higher charge states, protons were placed on both the histidine and carboxy moieties. For the lower charge state, one of the additional protons was removed from either the C- terminus or Rh575 carboxy moiety, or from histidine.

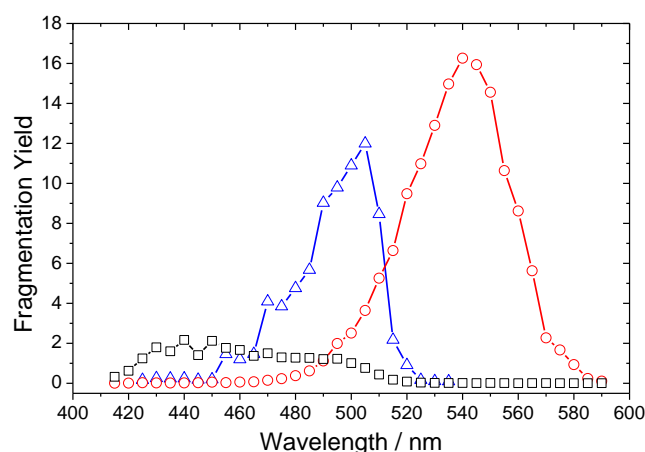


Figure 1. Action spectra of mass-selected (QSY7)⁺ (red circles), (rh575)⁺ (black squares) and (rh575-AAK-rh575)²⁺ (blue

triangles). Fragmentation yields are calculated from data measured in comparable experimental conditions and normalized with respect to the laser power.

Additionally, the two possible doubly grafted species discussed above (donor or acceptor grafted at the N-terminus) were considered. Two observables were extracted from these calculated structures in order to compare to the experimental measurements. The CCSs for simulated structures were calculated in the Mobcal suite of programs using the trajectory method with standard parameters.⁴⁴ The inter-chromophore distance was also extracted calculated as the minimum distance between any two atoms (excluding hydrogen) in the optically active portion of the chromophores (defined as the xanthene moiety plus the side chains).

Results and Discussion

Various processes are involved in action-FRET: the resonant energy transfer itself, as well as the competing radiative and non-radiative relaxation mechanism of both acceptor and donor chromophore. Thus, FRET relies on the choice of a suitable chromophore pair. In order to observe FRET in solution, the chromophores must have clearly resolved absorption bands and there must be a significant overlap of the donor fluorescence spectrum and acceptor absorption spectrum.

Moreover, the resonant energy transfer must happen on a shorter time-scale than the relaxation of the donor chromophore. Similar constraints exist for action-FRET in the gas phase, with the additional constraints that the acceptor chromophore must have a fragmentation pattern that is specific to electronic excitation and that is different from statistical fragmentation that occurs after heating (for example by CID or IRMPD). Therefore acceptor fragmentation must happen on a shorter time-scale than fluorescence and the statistical redistribution of the energy over the entire molecule. Thus, in the doubly grafted species, by monitoring the laser-induced

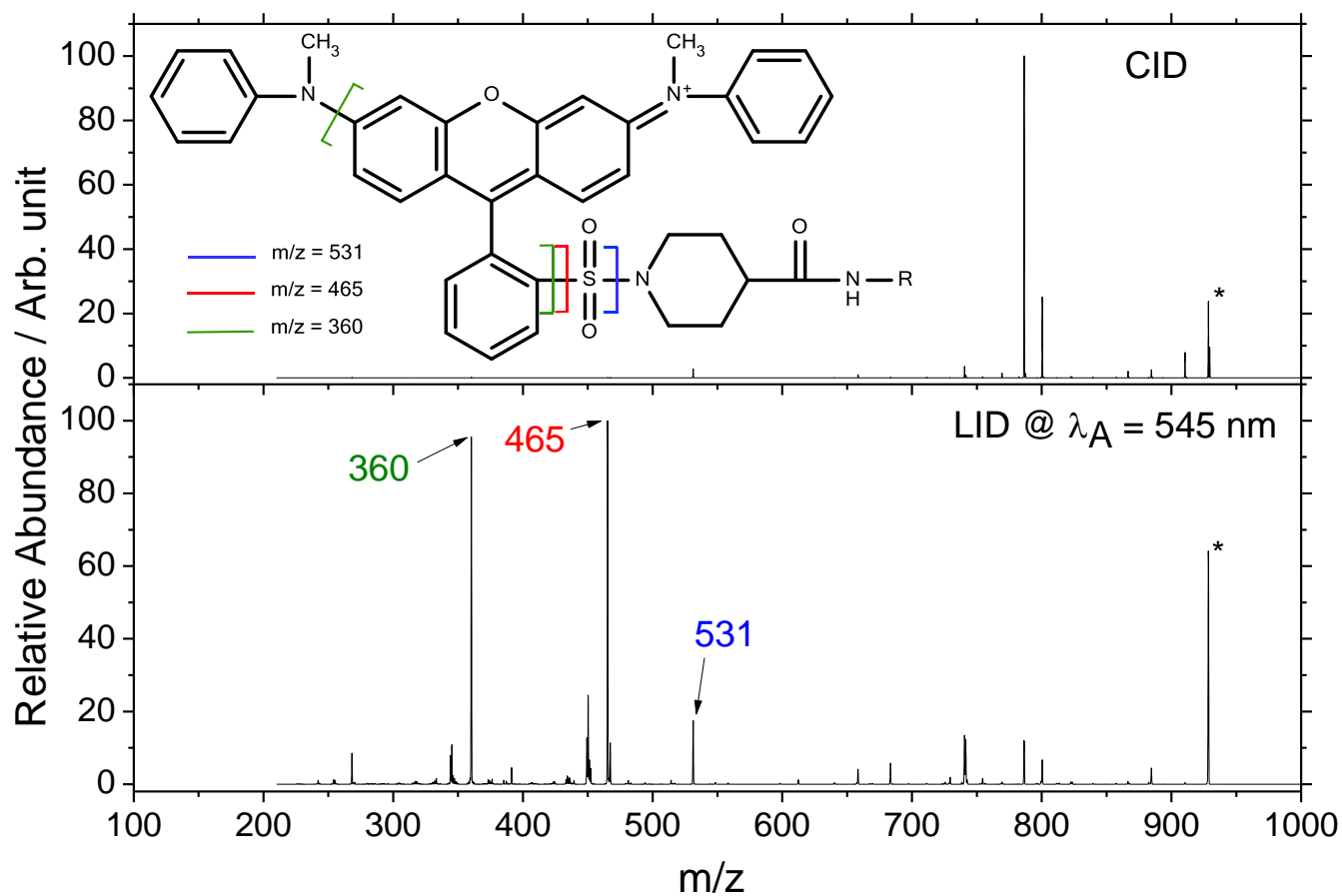


Figure 2. Mass spectra of mass-selected (QSY7-AAK)⁺ ions following CID (top panel) and LID at $\lambda_A = 545$ nm (bottom panel). The asterisk denotes the precursor ion. The top panel shows the structure of the (QSY7)⁺ ion, the R group representing the grafting location onto the peptide. The solid lines indicate the bonds broken to give rise to the major fragments observed in the LID mass spectrum.

dissociation (LID), we conclude that the observation of two absorption bands is due to FRET. It is also important to show that the strength of the observed action-FRET depends on the distance between the two chromophores.

Figure 1 shows the action spectra for mass-selected (rh575)⁺ (black squares) and (QSY7)⁺ (red circles), measured as total fragmentation yield. There is an obvious difference in the amplitude of the fragmentation yield of the two chromophores. Since rh575 has a high quantum yield (0.83 in ethanol) the primary relaxation mechanism can be expected to be fluorescence at the maximum of absorption, which has been shown to be $\lambda = 495$ nm in the gas phase.^{39,45} Hence the action spectrum in this case is weak due to fragmentation being a relatively minor relaxation mechanism, and thus the expected absorption maximum is not observed. As QSY7 is a dark quencher, fluorescence is not available as a relaxation mechanism and hence it fragments efficiently. In both cases, the fragmentation yield was measured as a function of power, and showed a quadratic dependence indicating that the fragmentation is a two photon process. This is consistent with previous study of the photo-fragmentation of rhodamines, which shows the same quadratic dependence at low power.³⁹ For measurement of all spectra presented here, the average power at each wavelength is kept between to 0.9 – 1.1 mW.

The blue triangles in figure 1 show the action spectrum of mass-selected (rh575-AAK-rh575)²⁺. It is a well-known property of rhodamines that there is a large reduction in the fluorescence quantum yield upon the formation of clusters of rhodamine molecules.⁴⁶ Hence there is a decrease in the importance of fluorescence as a relaxation mechanism, and a concurrent increase in the fragmentation yield is observed for (rh575-AAK-rh575)²⁺. This confirms the interpretation that the non-observance of the expected absorption maximum in the fragmentation yield of (rh575)⁺ is explained by the competition of fluorescence and fragmentation. It also suggests that the action spectrum of (rh575-AAK-rh575)²⁺ can be used as a proxy for the absorption spectrum of (rh575)⁺. Indeed, the position of the peak of $\lambda = 505$ nm for (rh575-AAK-rh575)²⁺ compares favorably with the value of $\lambda = 495$ nm found in previous *in vacuo* measurements.^{18,39} As a conclusion of the action spectroscopy studies, rh575 and QSY7 satisfy the first condition required for FRET; that the absorption bands are clearly distinguished, with absorption maxima of $\lambda_D = 505$ nm and $\lambda_A = 545$ nm respectively.

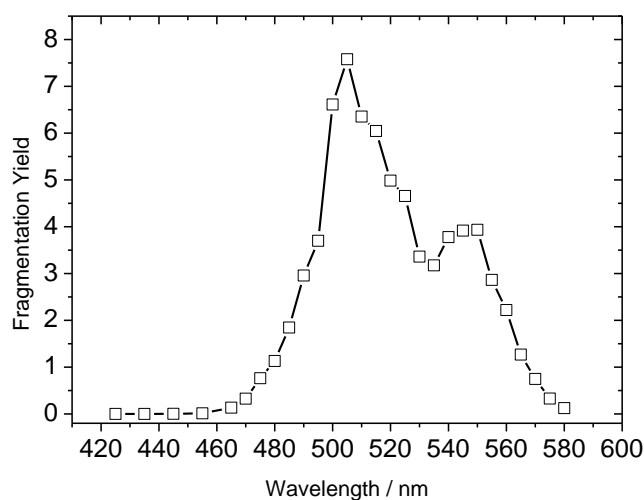


Figure 3. The action spectrum of mass-selected (rh575-AAK-QSY7)²⁺. The fragmentation yield here has been determined using only the LID-specific fragments as shown in figure 2.

Additionally, donor (rh575) emission as observed in the gas phase³⁹ and acceptor (QSY7) absorption spectra show a large overlap. Thus these two chromophores are well suited for FRET in the gas phase.

It must still be established that the fragmentation observed for the acceptor chromophore is LID-specific, so that one can discriminate the origin of the excitation. Figure 2 shows the mass spectra of mass-selected (AAK-QSY7)⁺ following CID (top) and LID at $\lambda_A = 545$ nm (bottom) respectively. There is clearly a large difference in the fragmentation pattern observed due to either heating or electronic excitation. The fragments observed in CID correspond to fragmentation of the peptide backbone. Conversely, the LID mass spectrum is dominated by two fragments at m/z 465 and 360, which correspond to the breaking of the S – C bond alone and combined breaking of the C – N bond between the xanthen and N-methylaniline moiety, see the inset of figure 2. These two latter fragments are not observed in CID and their observation is thus a clear signature that QSY7 has been electronically excited. It is therefore possible to follow FRET by measuring the relative intensity of these fragments as a function of wavelength for the doubly grafted peptides.

Figure 3 shows the result of this procedure for mass selected (rh575-AAK-QSY7)²⁺, giving an action spectrum where only the LID-specific acceptor fragments noted above are monitored. If there were no energy transfer, the same action spectrum as the one shown in figure 1 for QSY7 would be

expected. However, there are clearly two bands present in the spectrum; one at 545 nm corresponding to absorption of the acceptor chromophore, and one at 505 nm which is in the region where the donor chromophore was found to absorb. Observation of the donor chromophore absorption band via measurement of fragments specific to electronic excitation of the acceptor chromophore is direct evidence for electronic energy transfer having occurred.

Considering the data presented in figures 1-3, it is possible to make some general comments about the relative time-scales of the processes occurring following photo-excitation. Firstly, the action spectrum of (rh575)⁺ ions indicates that fluorescence from the excited state occurs on a shorter time-scale than either photo-fragmentation or internal vibrational redistribution (IVR), which is in full agreement with the high fluorescence quantum yield and a fluorescence lifetime of 5.65 ± 0.04 ns in vacuo.⁴⁷ Secondly, the high fragmentation yields observed in (AAK-QSY7)⁺ and the large difference in the observed fragmentation following CID and LID indicates that photo-fragmentation of (QSY7)⁺ occurs on a shorter time-scale than IVR. Finally, the observation of FRET in (rh575-AAK-QSY7)²⁺ indicates that FRET must occur on a shorter time-scale than fluorescence of (rh575)⁺, and again that the subsequent photo-fragmentation of (QSY7)⁺ must occur on a shorter time-scale than IVR. These results are completely consistent with previous fluorescence lifetime measurements of donor-peptide-acceptor systems.¹⁸ An additional important point to note is that the rate of IVR will increase as the length of the peptide is increased. As system size increases there, competition between IVR and direct photo-fragmentation of the acceptor chromophore may arise. As a consequence of this competition, the overall LID-specific fragmentation intensity can be expected to decrease relative to the intensity of the statistical fragments. This competition between IVR and photo-fragmentation will exist as soon as the energy is localized on the acceptor chromophore regardless of the origin of this energy: photo-fragmentation following FRET or following direct absorption will be equally affected. Therefore, if the FRET-mediated photo-fragmentation of the acceptor chromophore is normalized by the direct photo-fragmentation, an IVR independent quantification of action-FRET can be effected.

This discussion lends itself to the following definition of the action-FRET efficiency. The absorption due to the acceptor chromophore is independent of the system in terms of peak position and shape, with a spectrum resembling that shown in figure 1 being recorded when the acceptor chromophore is individually grafted onto each of the peptides used.

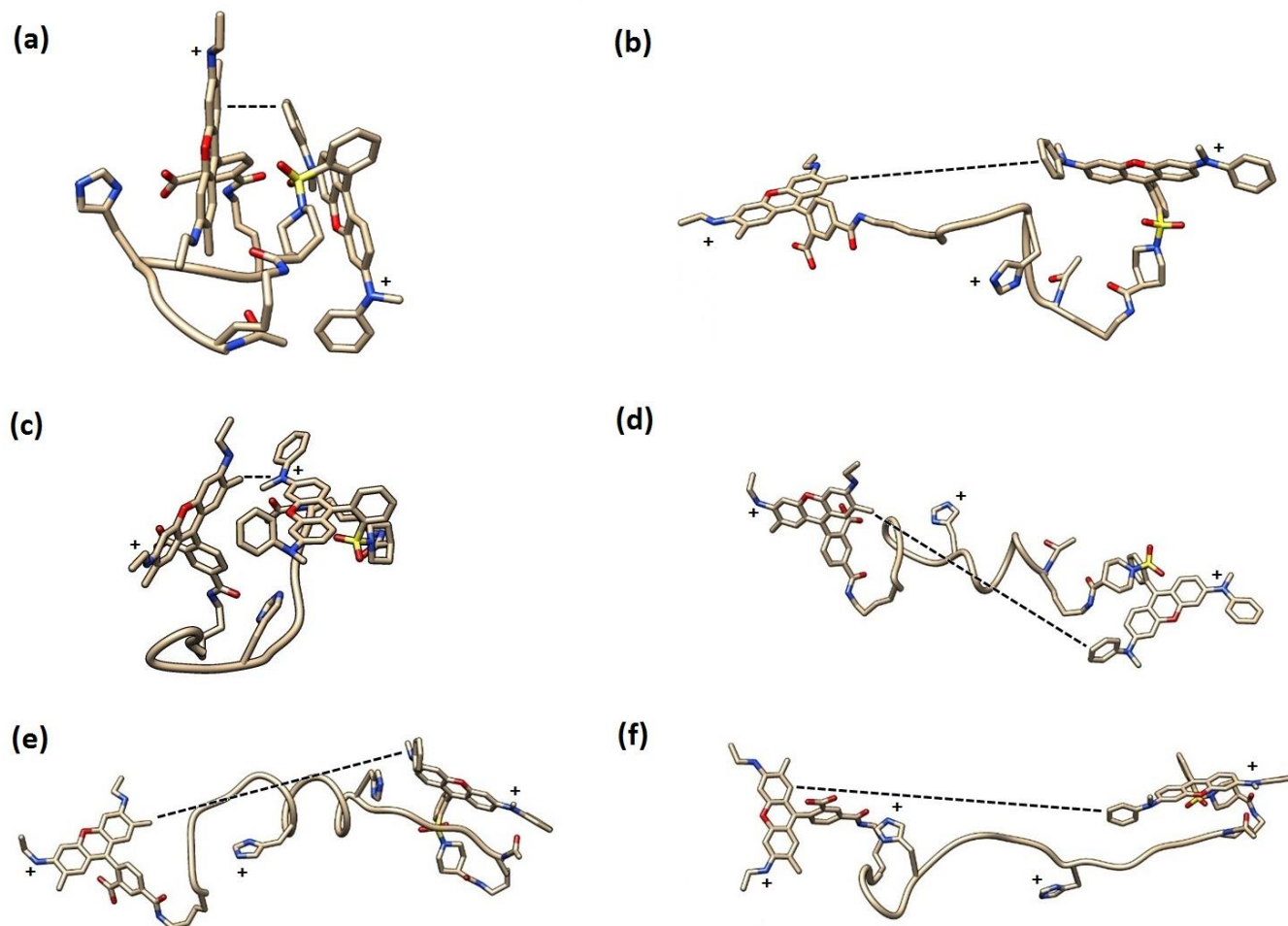


Figure 4. Lowest energy MCM structures for (a) (Rh575-KA₂HA₂K-QSY7)²⁺, (b) (Rh575-KA₂HA₂K-QSY7)³⁺, (c) (Rh575-KA₅HA₅K-QSY7)²⁺, (d) (Rh575-KA₅HA₅K-QSY7)³⁺, (e) (Rh575-KA₅HA₅HA₅K-QSY7)³⁺ and (f) (Rh575-KA₅HA₅HA₅K-QSY7)⁴⁺. The positions of the positive charges for each species are indicated on the figure. The dashed line shows the minimum separation of the chromophores and corresponds to the minimum distance between any two heavy atoms on the optically active region of the chromophore.

Thus, it is possible to take the ratio of the area of the peaks due to the donor and acceptor absorptions as a relative measure of the FRET efficiency. When this procedure is performed on the data for (rh575-AAK-QSY7)²⁺ (see figure S8) a value of 1.75 ± 0.34 is obtained, where the error is determined from the error in the fit. Measurements of the action spectra and an identical fitting procedure were performed on doubly grafted KA₂HA₂K, KA₅HA₅K, and KA₅HA₅HA₅K (see figures S9 – S14). Two charge states were observed in each case; 2+ and 3+ for (rh575-KA₂HA₂K-QSY7) and (rh575-KA₅HA₅K-QSY7) and 3+ and 4+ for (rh575-KA₅HA₅HA₅K-QSY7). Values of the FRET efficiency between 0.40 – 2.25 were measured for these species.

To investigate the relationship between the FRET efficiency and the chromophore separation – and hence the structure of the peptides – an independent determination of the structure of the doubly grafted peptides was obtained by measurement of the collision cross sections (CCS) using ion mobility spectrometry (IMS) and use of Monte Carlo-minimization (MCM) simulations for each charge state of the doubly grafted peptides, see table 1 and figure 4. It was not possible to measure experimentally the CCS values for the largest peptide

KA₅HA₅HA₅K due to a low total ion signal. Examination of the IMS profiles suggests a single conformational family is present for each of the systems studied, which is consistent with the observation of a single low energy conformational family in the MCM data. These conformational families possess the same peptide backbone structure, but differ in the orientation of the chromophores. To account for these conformational families, average values for the cross section and minimum chromophore separation - weighted by the relative energy of each conformer - were used. It is also important to note that the calculations for both doubly grafted species (rh575-peptide-QSY7) and (QSY7-peptide-rh575) were performed, and in each case the peptide backbone structure of the lowest energy

Table 1. Experimental and calculated collision cross sections and FRET efficiency of doubly grafted peptides.

peptide	charge	MCM CCS Å ²	Exp. CCS Å ²	FRET efficiency
AAK	2+	337 ± 4	324	1.75 ± 0.12
KA ₂ HA ₂ K	3+	445 ± 3	508	1.02 ± 0.25

	2+	374 ± 3	377	1.72 ± 0.44
KA ₅ HA ₅ K	3+	518 ± 7	557	0.85 ± 0.21
	2+	452 ± 4	467	2.25 ± 0.45
KA ₅ HA ₅ HA ₅ K	4+	624 ± 5		0.40 ± 0.10
	3+	635 ± 4		0.61 ± 0.11

conformational family was identical. Examination of table 1 shows that there is in general a good agreement between the calculated and experimental CCS values for each species. It should be noted that there is an underestimation of the CCS for the 3+ charge state of the peptides, suggesting that the calculated structures are too compact which will lead to an underestimation of the minimum chromophore separation. Nonetheless, it is clear that each doubly grafted peptide becomes more extended as the charge state is increased from 2+ to 3+. This is consistent with the intuitive expectation that Coulomb repulsion would cause unfolding at higher charge states, causing a concurrent increase in the chromophore separation. Indeed, in the 2+ charge state of the doubly grafted peptides, it is the two chromophores that carry the positive charges. In the 3+ charge state, the proton is added to the histidine side chain and the additional Coulomb repulsion forces the chromophores apart (see figure 4 (a) – (d)). In the case of doubly grafted KA₅HA₅HA₅K the 3+ and 4+ charge states are observed, corresponding to protonation of one and two histidine side chains respectively (figure 4 (e) and (f)). Both charge states are calculated to have an extended structure with the main difference being the uncoiling of the helical motif of the 5 alanine residues situated between the two histidine residues. It can be concluded from the comparison of experimental and calculated CCS that the calculated structures are representative of the doubly grafted peptides, and thus we can examine the dependence of the FRET efficiency on the minimum chromophore separation – as defined above.

Figure 5 shows the FRET efficiency against minimum chromophore separation for all doubly grafted species examined (see table 1 for the numerical values). It is clear that there is a monotonic decrease in the FRET efficiency as the separation of the chromophores is increased. The FRET efficiency of the higher charge state is consistently less than that of the lower charge state, for each peptide size, which is consistent with the CCS data presented above.

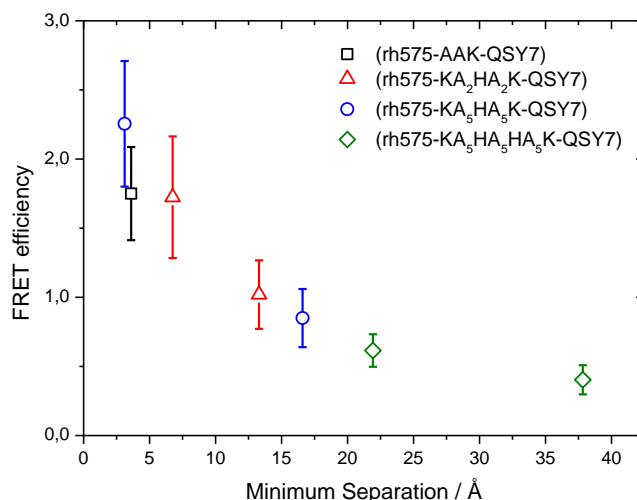


Figure 5. FRET efficiency versus average value of the minimum chromophore separation for the different charge states of doubly grafted AAK (squares), KA₂HA₂K (triangles), KA₅HA₅K (circles) and KA₅HA₅HA₅K (diamonds).

In particular the large change in structure - from globular to extended - that is observed with the addition of a proton for doubly grafted KA₂HA₂K and KA₅HA₅K leads to an equally large change in the FRET efficiency; from 1.72 ± 0.44 to 1.02 ± 0.25 in KA₂HA₂K and from 2.25 ± 0.45 to 0.85 ± 0.21 in KA₅HA₅K.

The situation for doubly grafted KA₅HA₅HA₅K is interesting as the MCM calculations suggest that there is not a large change in the global shape as the charge state is increased from 3+ to 4+. This is reflected in the small change calculated values of the CCS from 624 Å² to 635 Å². However, there is a proportionally greater change in the value of the FRET efficiency; 0.61 ± 0.11 for the 3+ and 0.40 ± 0.10 for the 4+ charge state respectively. This suggests that the action-FRET is more sensitive to such local changes in structure – in this case the uncoiling of the central five alanine residues – than is IMS, and therefore the two techniques are able to provide complementary information. Overall, these data are in agreement with previous results on the structure of gas phase multi-charged poly-alanines, showing that chromophores have limited influence on the structure of the peptides.^{48,49}

A final point to note is that it is possible to measure the action FRET by performing measurement of the LID spectrum at only 2 wavelengths; λ_D and λ_A . In such a case, the FRET efficiency would be defined as the ratio of the fragmentation yield of acceptor fragments measured at λ_D and λ_A . If this procedure is performed on the data presented in this paper, identical trends are observed.

Conclusion.

We have proposed a scheme for the measurement of FRET in the gas phase using a method based only on fragment ion detection. The principal features that would have to be identified for such an action-FRET scheme were discussed and subsequently shown experimentally. A dark-quenching chromophore, QSY7, was identified and its fragmentation characterized to show that there were fragments specific to electronic excitation. A suitable fluorescent donor chromophore, rh575, was identified and characterized.

Measurement of the action spectrum of the two chromophores both grafted onto the simple tripeptide AAK showed that the absorption maximum of rh575 is observed via measurement of the fragments specific to the electronic excitation of QSY7. Thus, it was possible to conclude that the energy had been transferred from the donor to acceptor chromophore. It was also possible to conclude that the FRET observed must occur on a shorter time-scale than both the fluorescence of the donor, and the internal vibrational redistribution of energy across the entire molecule. It was also possible to define an IVR-independent quantification of the FRET efficiency considering the photo-fragmentation efficiency following FRET and direct absorption of the acceptor chromophore.

This definition of the FRET efficiency – taken as the ratio of the area of the peaks in the action spectrum due to absorption of the donor and acceptor chromophores – was used in conjunction with measurements of the collision cross section via IMS and MCM simulations on a series of poly-alanine based peptides containing between 7 and 19 amino acids. It was shown that there is a clear dependence on the magnitude of the FRET efficiency observed with the separation of the chromophores in each the system studied. Comparison with MCM simulations showed that the FRET efficiency is well correlated with an increase in the separation of donor and acceptor chromophores. Hence the action-FRET methodology set out in the paper is suitable for gas-phase studies of the structure of biomolecules and provides orthogonal information to IMS measurements as it is sensitive to a distance between two defined parts of the molecular ion, while IMS is sensitive to the global shape. The action-FRET methodology provides a significant advance in the study of the conformation and structure of gas-phase molecular ions. This method therefore has a strong potential in native MS as part of a global approach in structural biology.

ASSOCIATED CONTENT

CID and LID mass spectra of singly and doubly grafted AAK; identification of the internal chromophore fragments; fitted raw action spectra for all doubly grafted species; MCM structures of doubly grafted 3 and 7 residue peptides; plot of FRET efficiency versus chromophore separation; tabulated form of the data shown in figure 5. This material is available free of charge via the Internet at <http://pubs.acs.org>.

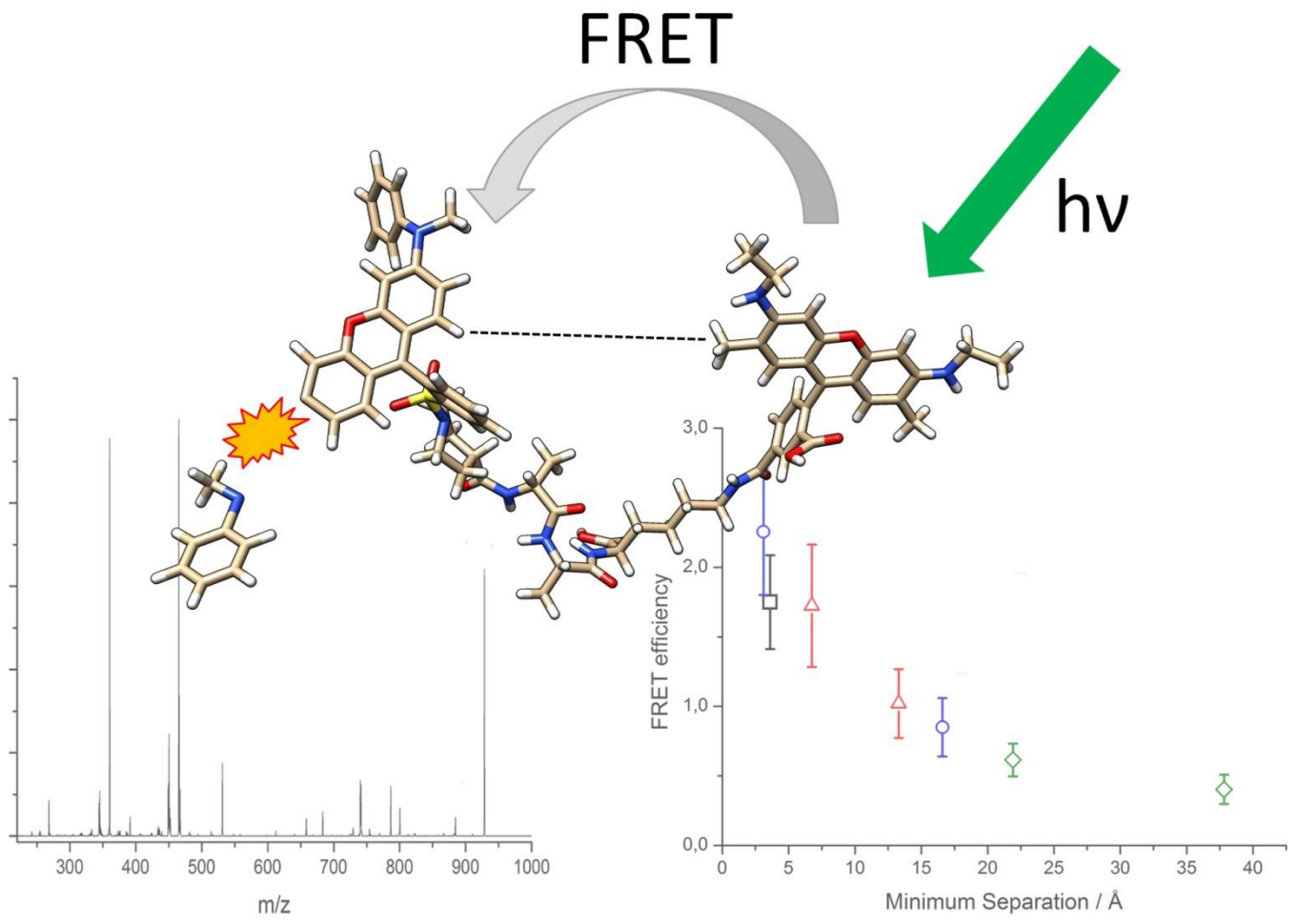
ACKNOWLEDGMENT

The research leading to these results has received funding from the European Research Council under the European Union's Seventh Framework Program (FP7/2007-2013 Grant agreement N°320659).

REFERENCES

- (1) Weiss, S. *Science* **1999**, *283*, 1676.
- (2) Selvin, P. R. *Nat. Struct. Bio.* **2000**, *7*, 730.
- (3) Schuler, B.; Lipman, E. A.; Eaton, W. A. *Nature* **2002**, *419*, 743.
- (4) Giepmans, B. N. G.; Adams, S. R.; Ellisman, M. H.; Tsien, R. Y. *Science* **2006**, *312*, 217.
- (5) Ruotolo, B. T.; Robinson, C. V. *Curr. Opin. in Chem. Biol.* **2006**, *10*, 402.
- (6) van den Heuvel, R. H.; Heck, A. J. R. *Curr. Opin. in Chem. Biol.* **2004**, *8*, 519.
- (7) Miranker, A.; Robinson, C. V.; Radford, S. E.; Aplin, R. T.; Dobson, C. M. *Science* **1993**, *262*, 896.
- (8) Heck, A. J. R. *Nat. Methods* **2008**, *5*, 927.
- (9) Vonhelden, G.; Wyttenbach, T.; Bowers, M. T. *Science* **1995**, *267*, 1483.
- (10) Sinz, A. *Mass Spectrom. Rev.* **2006**, *25*, 663.
- (11) Konermann, L.; Pan, J. X.; Liu, Y. H. *Chem. Soc. Rev.* **2011**, *40*, 1224.
- (12) Breuker, K.; Oh, H. B.; Horn, D. M.; Cerda, B. A.; McLafferty, F. W. *J. Am. Chem. Soc.* **2002**, *124*, 6407.
- (13) Bleiholder, C.; Dupuis, N. F.; Wyttenbach, T.; Bowers, M. T. *Nat. Chem.* **2011**, *3*, 172.
- (14) Bush, M. F.; Hall, Z.; Giles, K.; Hoyes, J.; Robinson, C. V.; Ruotolo, B. T. *Anal. Chem.* **2010**, *82*, 9557.
- (15) Uetrecht, C.; Rose, R. J.; van Duijn, E.; Lorenzen, K.; Heck, A. J. R. *Chem. Soc. Rev.* **2010**, *39*, 1633.
- (16) Danell, A. S.; Parks, J. H. *Int. J. Mass Spectrom.* **2003**, *229*, 35.
- (17) Dashtiev, M.; Azov, V.; Frankevich, V.; Scharfenberg, L.; Zenobi, R. *J. Am. Soc. Mass Spectr.* **2005**, *16*, 1481.
- (18) Talbot, F. O.; Rullo, A.; Yao, H.; Jockusch, R. A. *J. Am. Chem. Soc.* **2010**, *132*, 16156.
- (19) Frankevich, V.; Guan, X. W.; Dashtiev, M.; Zenobi, R. *Eur. J. Mass Spectrom.* **2005**, *11*, 475.
- (20) Iavarone, A. T.; Meinen, J.; Schulze, S.; Parks, J. H. *Int. J. Mass Spectrom.* **2006**, *253*, 172.
- (21) Iavarone, A. T.; Patriksson, A.; van der Spoel, D.; Parks, J. H. *J. Am. Chem. Soc.* **2007**, *129*, 6726.
- (22) Shi, X. G.; Duft, D.; Parks, J. H. *J. Phys. Chem. B* **2008**, *112*, 12801.
- (23) Frankevich, V.; Chagovets, V.; Widjaja, F.; Barylyuk, K.; Yang, Z. Y.; Zenobi, R. *Phys. Chem. Chem. Phys.* **2014**, *16*, 8911.
- (24) Bowers, W. D.; Delbert, S. S.; Hunter, R. L.; McIver, R. T. *J. Am. Chem. Soc.* **1984**, *106*, 7288.
- (25) Vanderhart, W. *J. Mass Spectrom. Rev.* **1989**, *8*, 237.
- (26) Dunbar, R. C. *Int. J. Mass Spectrom.* **2000**, *200*, 571.
- (27) Brodbelt, J. S. *Chem. Soc. Rev.* **2014**, *43*, 2757.
- (28) MacAleese, L.; Maitre, P. *Mass Spectrom. Rev.* **2007**, *26*, 583.
- (29) Drayss, M. K.; Blunk, D.; Oomens, J.; Polfer, N.; Schmuck, C.; Gao, B.; Wyttenbach, T.; Bowers, M. T.; Schafer, M. *Int. J. Mass Spectrom.* **2009**, *281*, 97.
- (30) Case, A. S.; Heid, C. G.; Western, C. M.; Crim, F. F. *J. Chem. Phys.* **2012**, *136*, 8.
- (31) Crampton, K. T.; Rathur, A. I.; Nei, Y. W.; Berden, G.; Oomens, J.; Rodgers, M. T. *J. Am. Soc. Mass Spectr.* **2012**, *23*, 1469.
- (32) Wyer, J. A.; Jensen, C. S.; Nielsen, S. B. *Int. J. Mass Spectrom.* **2011**, *308*, 126.
- (33) Yao, H.; Jockusch, R. A. *J. of Phys. Chem. A* **2013**, *117*, 1351.
- (34) Klaerke, B.; Holm, A. I. S.; Andersen, L. H. *Astron. Astrophys.* **2011**, *532*, 5.
- (35) Hansen, C. S.; Kirk, B. B.; Blanksby, S. J.; O'Hair, R. A. J.; Trevitt, A. J. *J. Am. Soc. Mass Spectr.* **2013**, *24*, 932.
- (36) Kirk, B. B.; Trevitt, A. J.; Blanksby, S. J.; Tao, Y. Q.; Moore, B. N.; Julian, R. R. *J. Phys. Chem. A* **2013**, *117*, 1228.
- (37) Macaleese, L.; Chirot, F.; Bazus, L.; Bertorelle, F.; Antione, R.; Lemoine, J.; Dugourd, P. In *ASMS Conference on Mass Spectrometry and Allied Topics*. Vancouver, 2012.
- (38) Enjalbert, Q.; Girod, M.; Simon, R.; Jeudy, J.; Chirot, F.; Salvador, A.; Antoine, R.; Dugourd, P.; Lemoine, J. *J. Anal. Bioanal. Chem.* **2013**, *405*, 2321.
- (39) Forbes, M. W.; Jockusch, R. A. *J. Am. Soc. Mass Spectr.* **2011**, *22*, 93.
- (40) Larraillet, V.; Antoine, R.; Dugourd, P.; Lemoine, J. *Anal. Chem.* **2009**, *81*, 8410.

- (41) Albrieux, F.; Calvo, F.; Chiro, F.; Vorobyev, A.; Tsybin, Y. O.; Lepere, V.; Antoine, R.; Lemoine, J.; Dugourd, P. *J. Phys. Chem. A* **2010**, *114*, 6888.
- (42) See the website at <http://dasher.wustl.edu/tinker>.
- (43) Halgren, T. A. *J. Comput. Chem.* **1996**, *17*, 490.
- (44) Mesleh, M. F.; Hunter, J. M.; Shvartsburg, A. A.; Schatz, G. C.; Jarrold, M. F. *J. Phys. Chem.* **1996**, *100*, 16082.
- (45) Arbeloa, F. L.; Arbeloa, T. L.; Lage, E. G.; Arbeloa, I. L.; Deschryver, F. C. *J. Photoch. Photobio. A* **1991**, *56*, 313.
- (46) McRae, E. G.; Kasha, M. *J. Chem. Phys.* **1958**, *28*, 721.
- (47) Nagy, A. M.; Talbot, F. O.; Czar, M. F.; Jockusch, R. A. *J. Photoch. Photobio. A* **2012**, *244*, 47.
- (48) Hudgins, R. R.; Jarrold, M. F. *J. Am. Chem. Soc.* **1999**, *121*, 3494.
- (49) Counterman, A. E.; Clemmer, D. E. *J. Phys. Chem. B* **2003**, *107*, 2111.



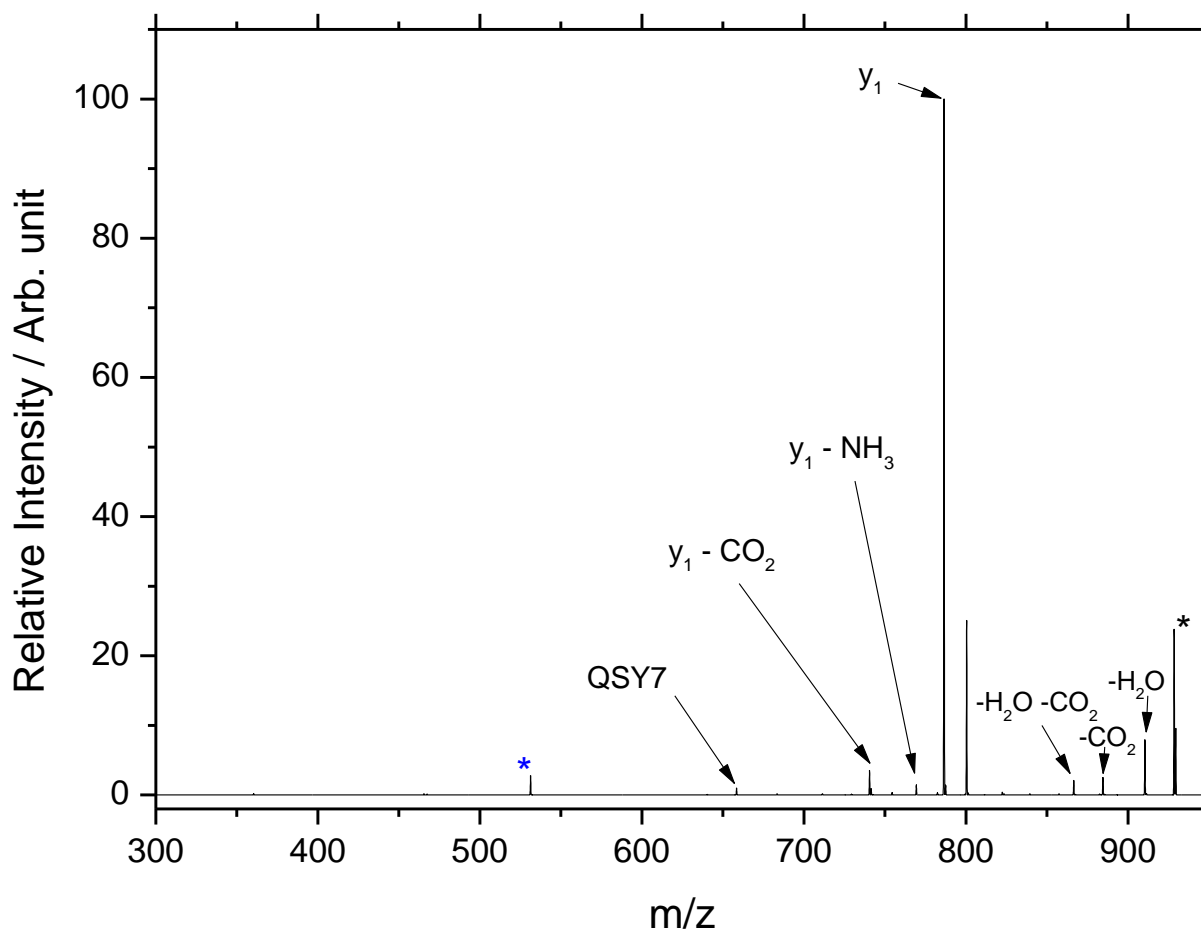


Figure S1. Mass spectrum following CID (NCE = 27) of mass-selected $(\text{QSY7-AAK})^+$, denoted with a black asterisk. The blue asterisk denotes a fragment due to internal chromophore fragmentation. The charge is located on the chromophore in all cases.

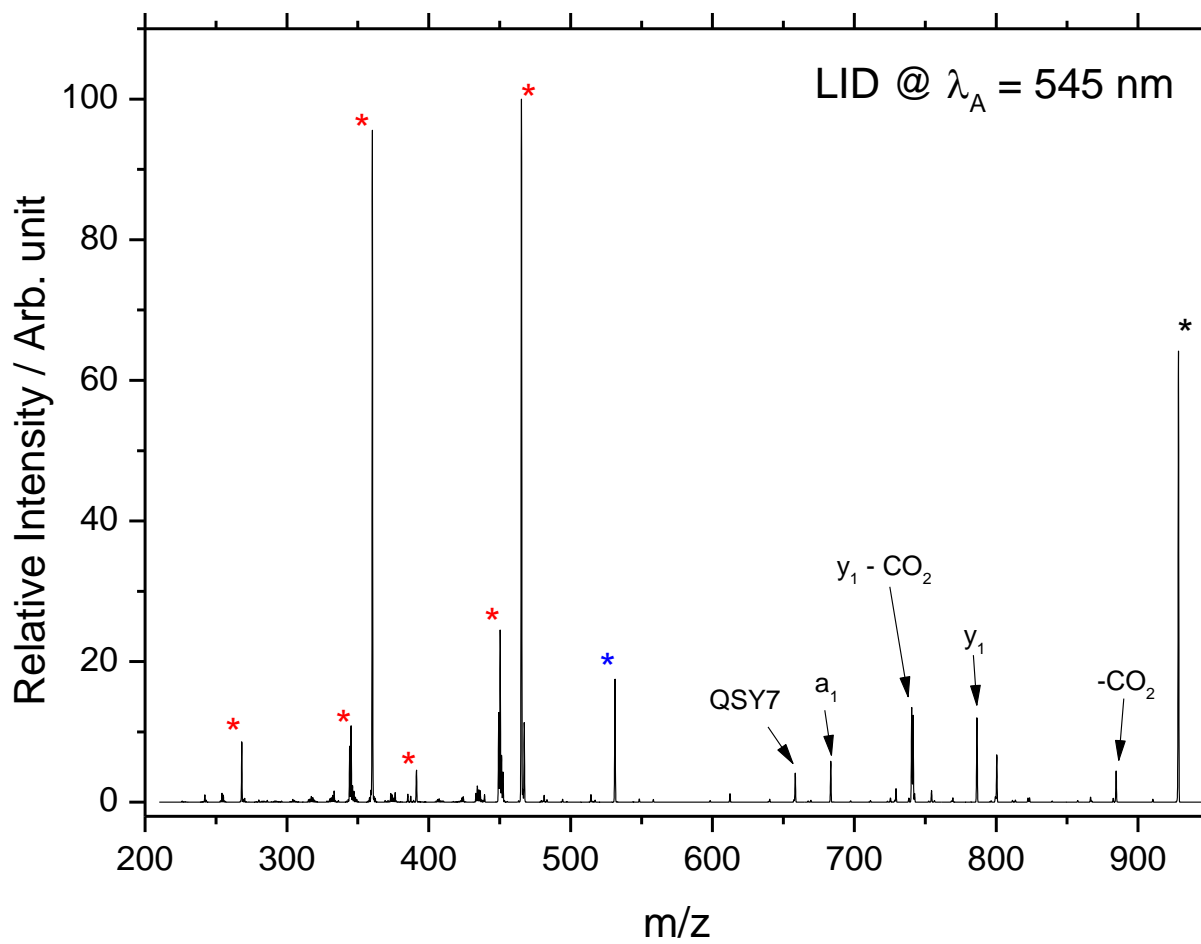


Figure S2. Mass spectrum following LID ($\lambda_A = 545\text{nm}$) of mass-selected (QSY 7-AAK)⁺, denoted with a black asterisk. The peaks highlighted with a red asterisks are internal chromophore fragmentation channels seen only in following electronic excitation. The peak highlighted with a blue asterisk is an internal chromophore fragmentation which is also seen in CID. The two major channels observed are m/z 465 and 360, see figure S7 for details.

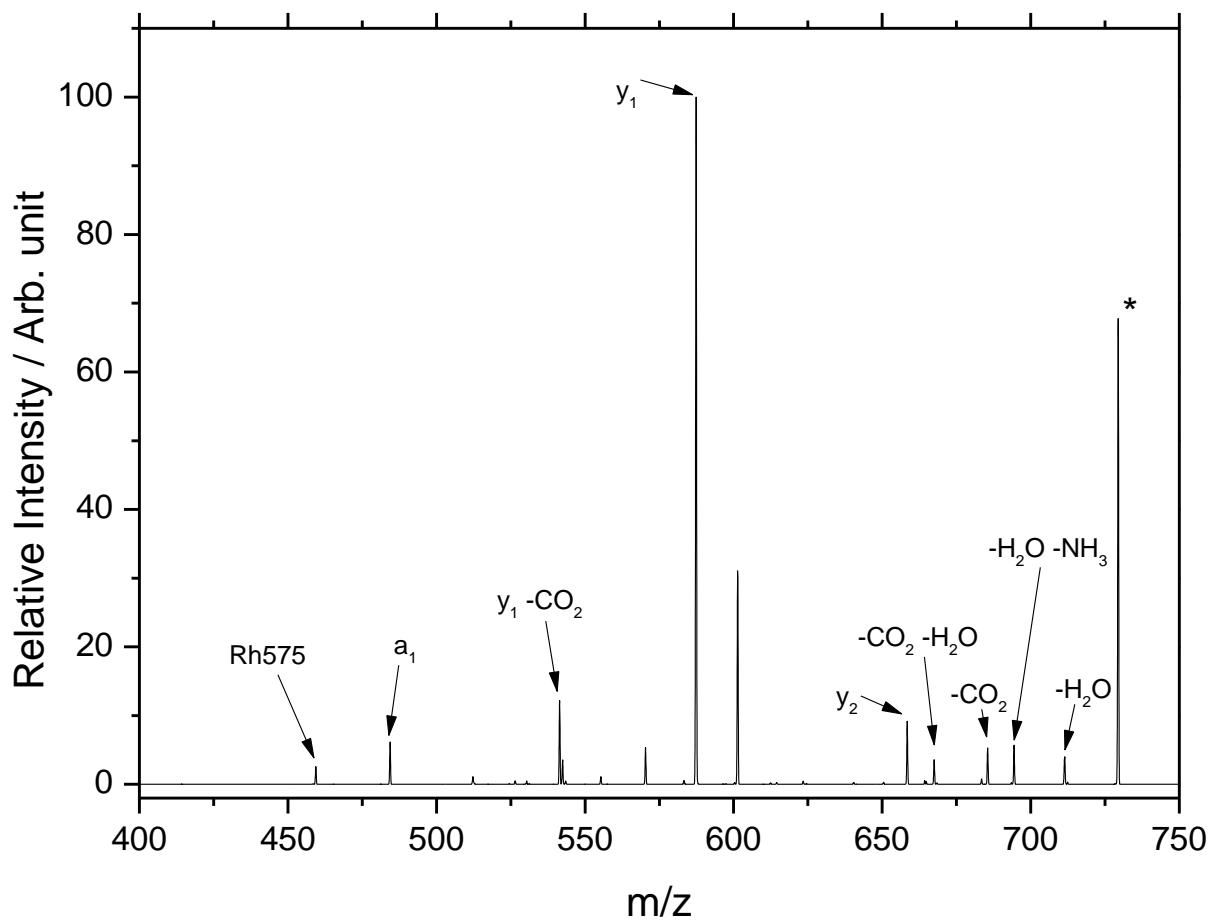


Figure S3. Mass spectrum following CID (NCE = 29) of mass-selected (rh575-AAK)⁺, denoted with a black asterisk. The charge is located on the chromophore in all cases.

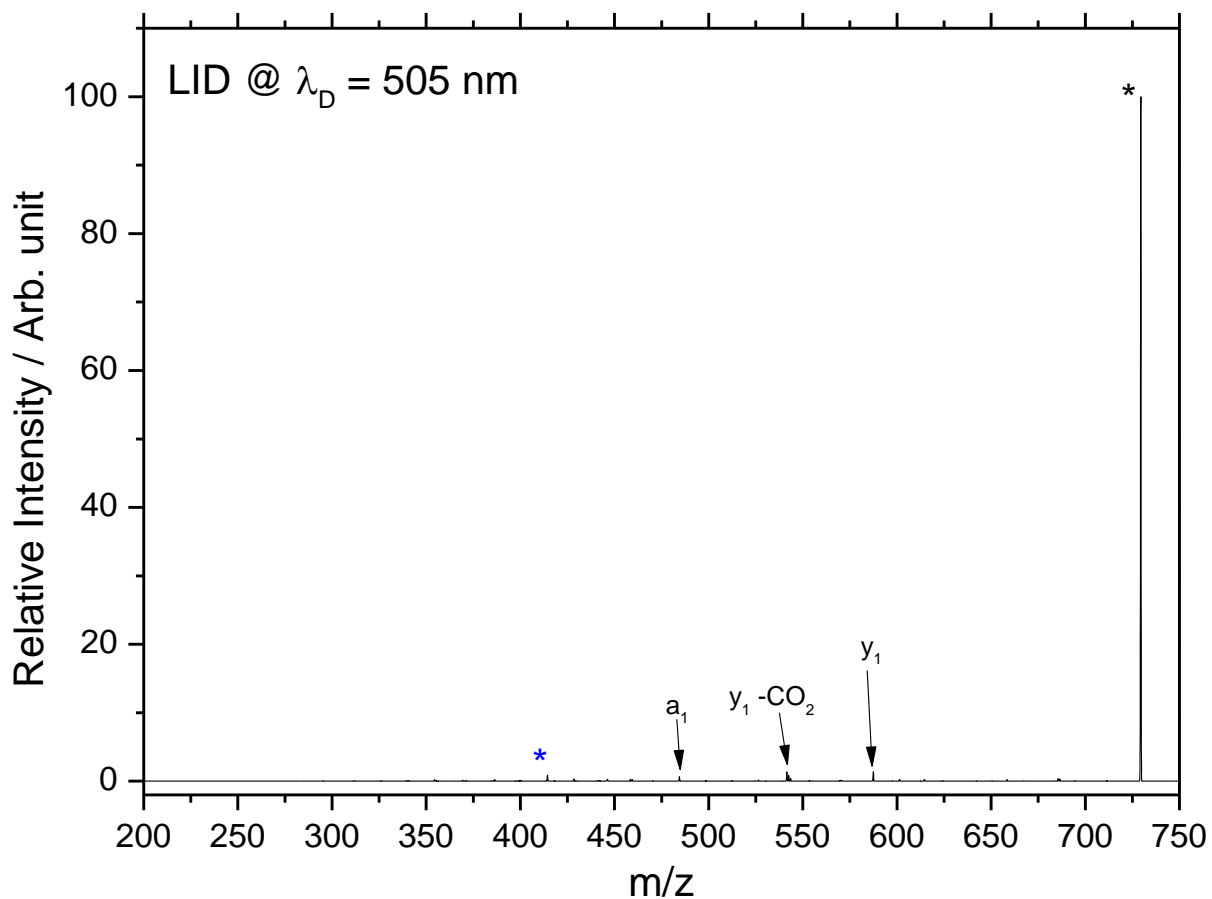


Figure S4. Mass spectrum following LID ($\lambda_D = 505$ nm) of mass-selected (rh575-AAK)⁺, denoted with a black asterisk. The absence of fragmentation following LID is due to the high fluorescence quantum yield of Rh575. The peak marked by the blue asterisk corresponds to an internal fragmentation of the rh575 chromophore, see figure S7.

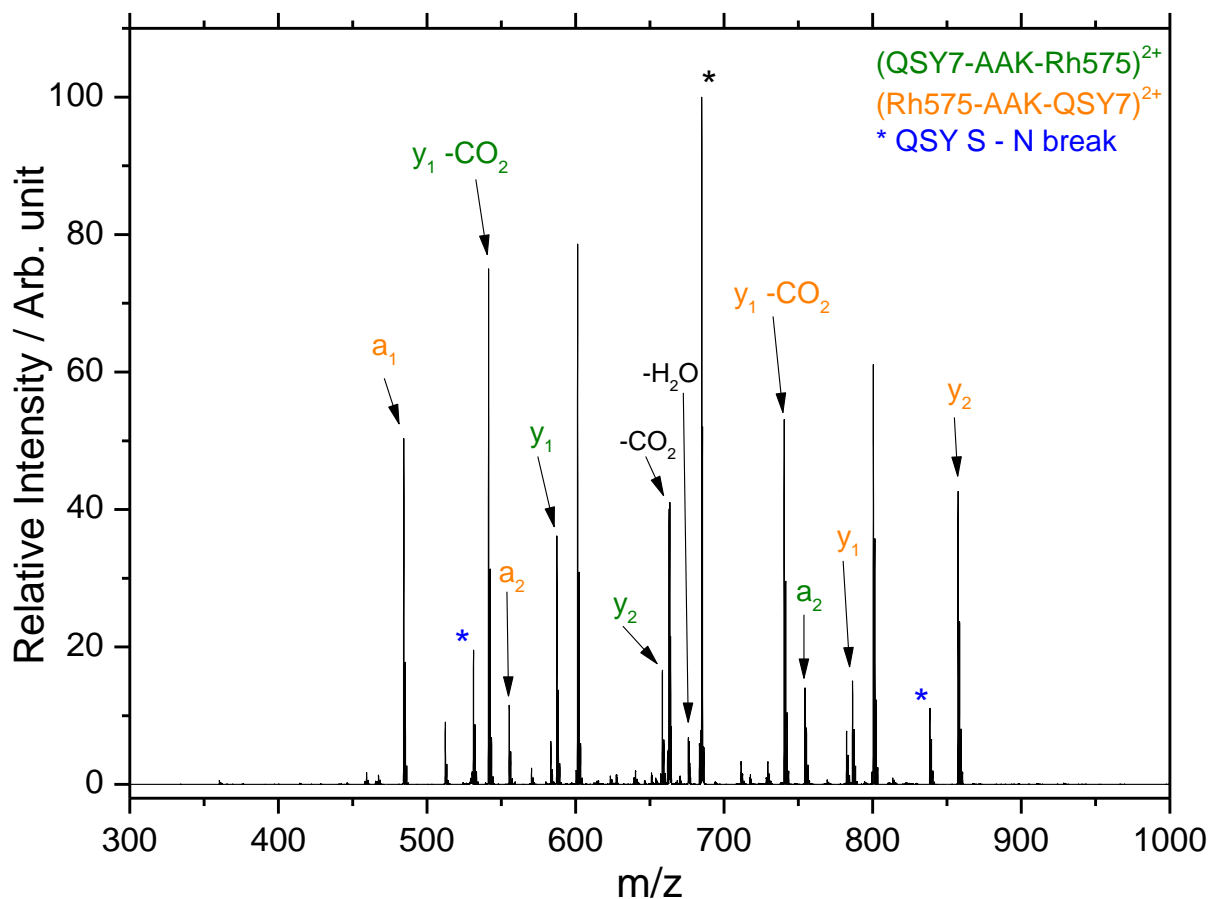


Figure S5. Mass spectrum following CID (NCE = 35) of mass-selected $(rh575\text{-AAK-QSY7})^{2+}$, denoted with a black asterisk. As the charges are located on the two chromophores, it is possible to distinguish the fragmentation of both doubly grafted species $(rh575\text{-AAK-QSY7})^{2+}$ (orange labels) and $(QSY\text{-AAK-rh575})^{2+}$ (green labels). It can be concluded that both species are present in the solution. The peaks marked with blue asterisks correspond to the internal fragmentation of QSY7 at the S – N bond, and it's concurrently produced ion.

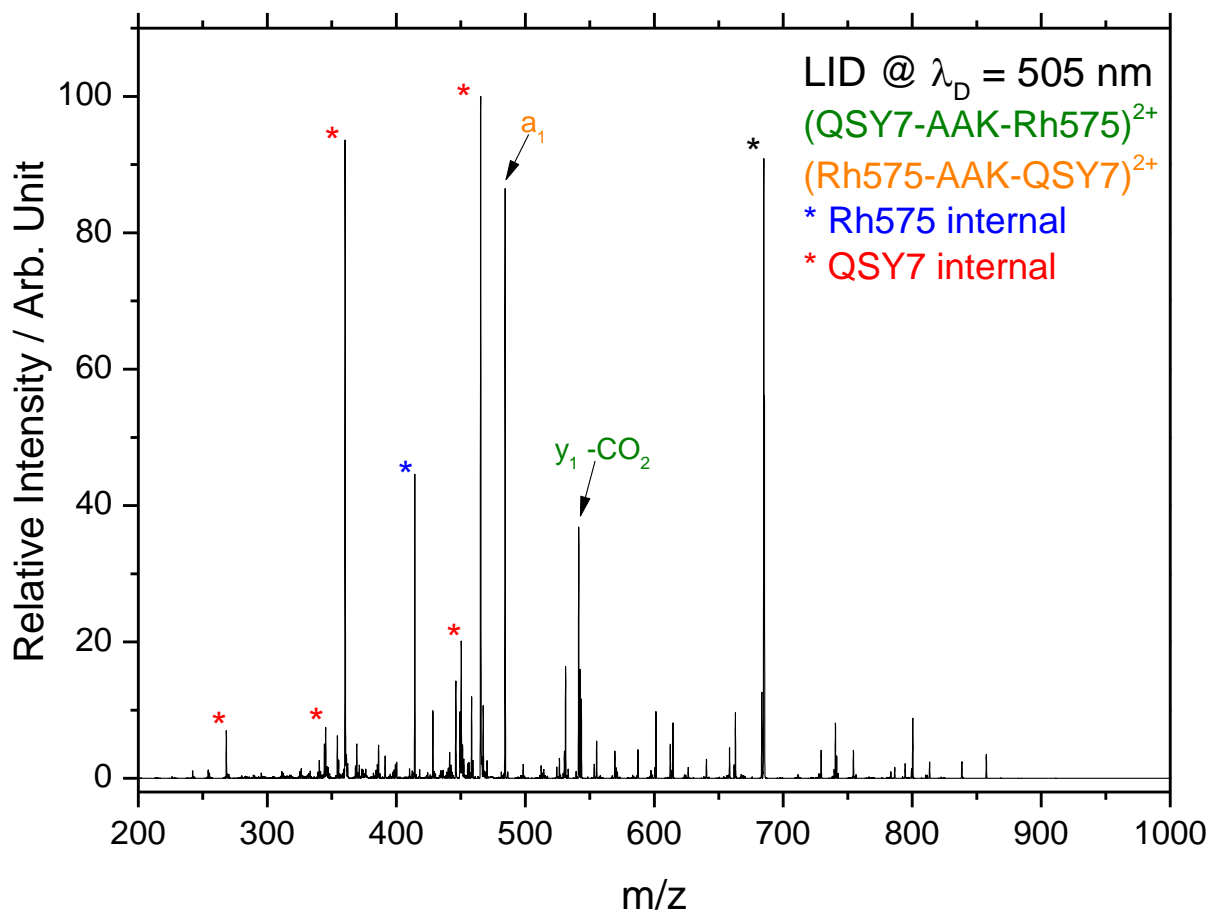


Figure S6. Mass spectrum following LID ($\lambda_D = 505$ nm) of mass-selected (rh575-AAK-QSY7)²⁺, denoted by a black asterisk. Labels of peaks due to peptide fragmentation shown above have not been replicated for clarity, excepting those of large intensity. The blue asterisks denote fragments not associated with LID specific fragmentation of QSY7. The peak at $m/z = 414$, assigned to an internal fragmentation of rh575, is also observed at $\lambda_A = 545$ nm. It is therefore likely that this is due to a secondary fragmentation process occurring in the ion partner of the internal QSY7 fragments, which are not observed. The peaks marked by red asterisks are LID-specific fragments of QSY7, and are due to the fragments used to monitor the resonant energy transfer from donor to acceptor chromophores.

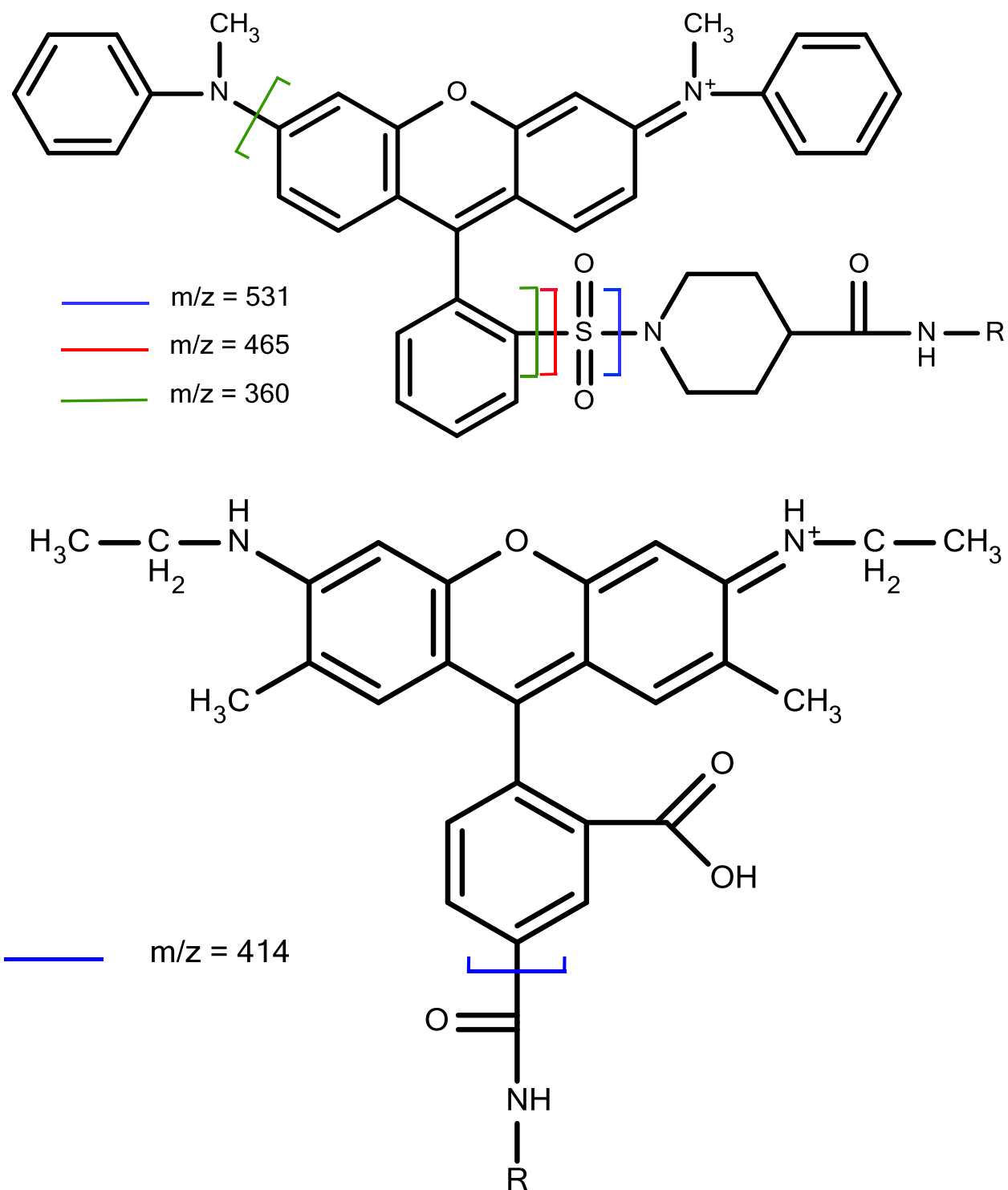


Figure S7. The major internal fragmentation pathways of QSY7 (top) and rh575 (bottom). The solid lines represent the bonds that break to form the fragment specified to the left in each case.

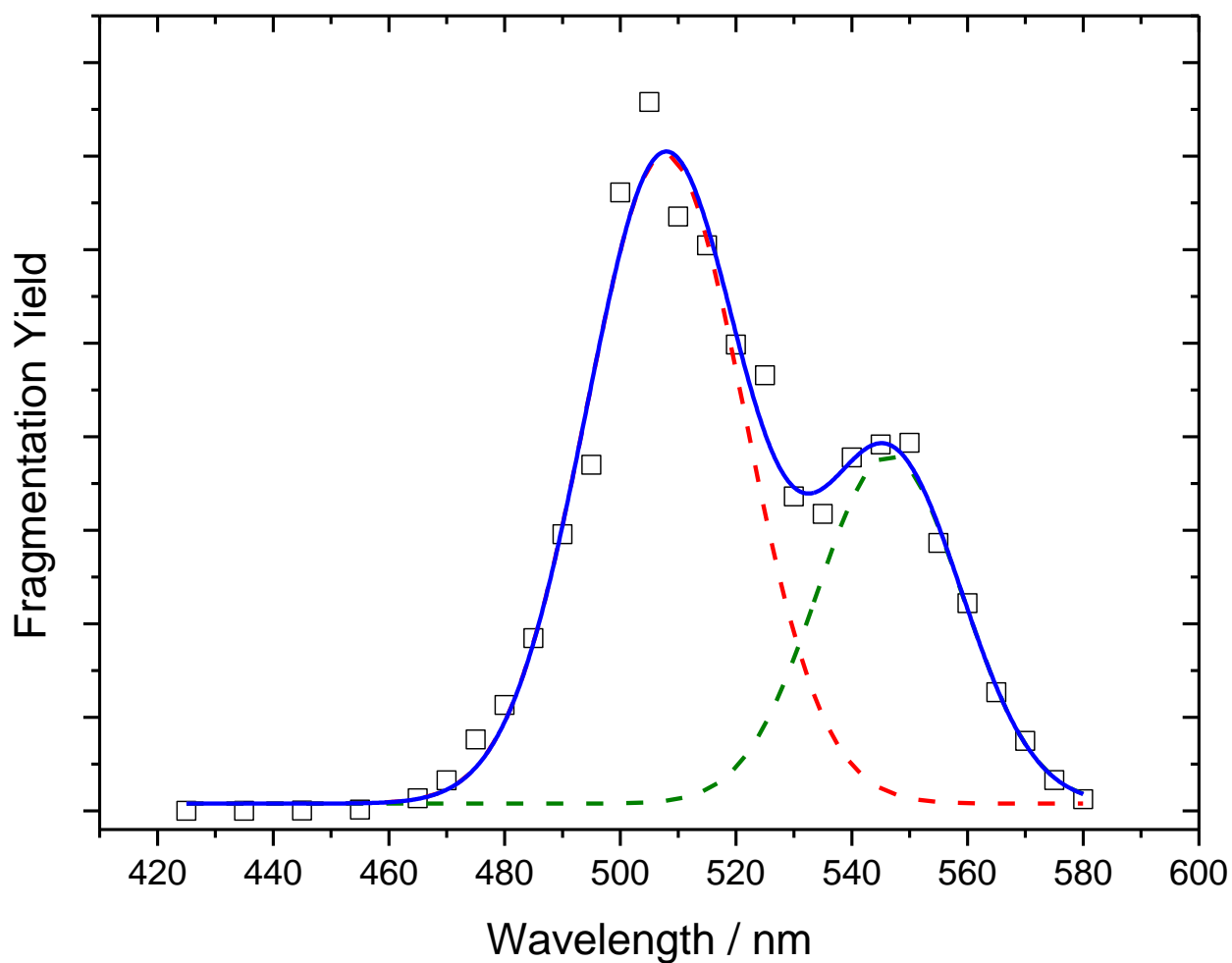


Figure S8. The fitted raw action spectrum of mass-selected $(\text{Rh575-AAK-QSY7})^{2+}$ (black squares). The dashed curves represent the fit to the QSY7 (green) and Rh575 (red) absorption bands. The solid blue curve represents the total fit.

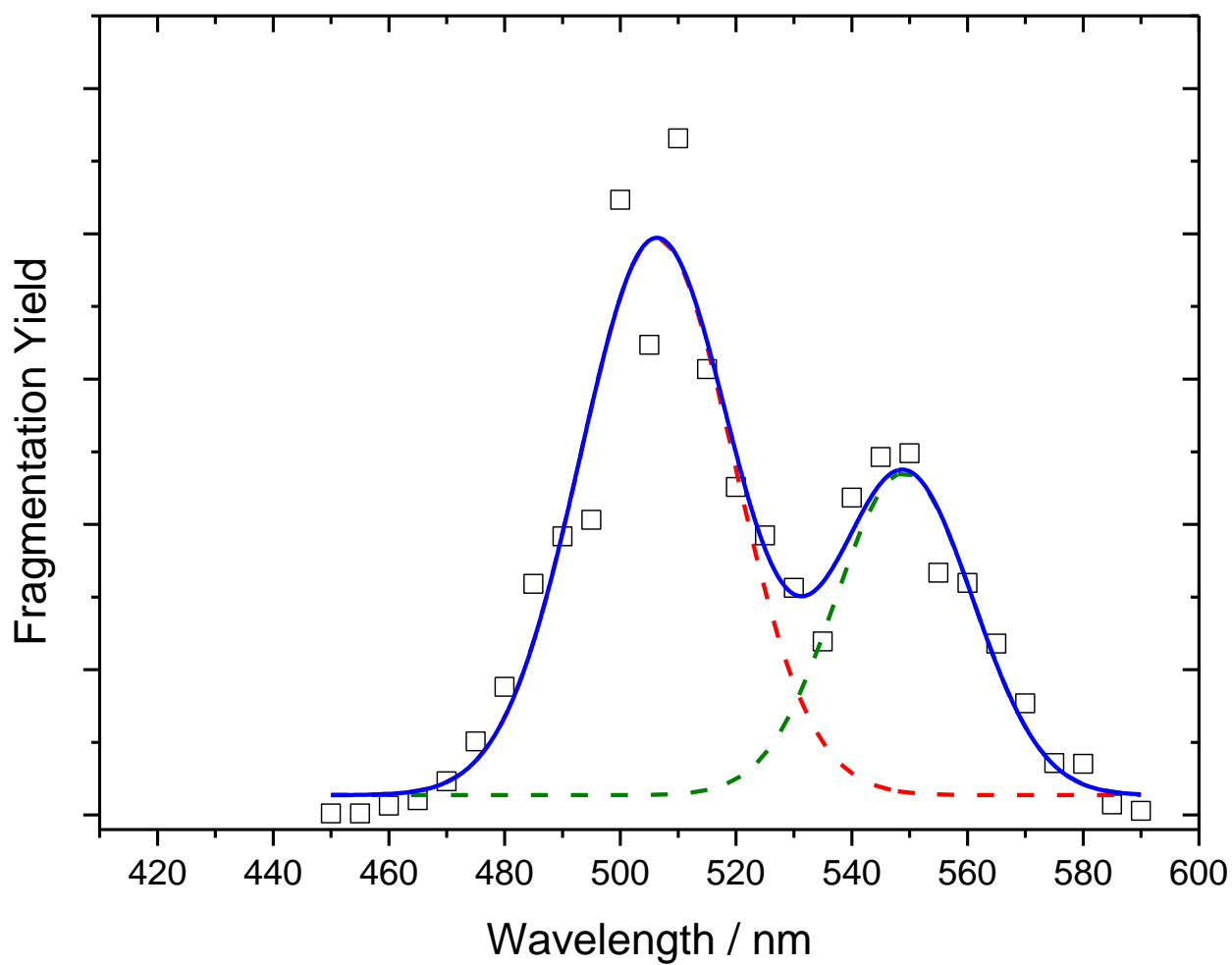


Figure S9. The fitted raw action spectrum of mass-selected $(\text{Rh575-KA}_2\text{HA}_2\text{K-QSY7})^{2+}$ (black squares). The dashed curves represent the fit to the QSY7 (green) and Rh575 (red) absorption bands. The solid blue curve represents the total fit.

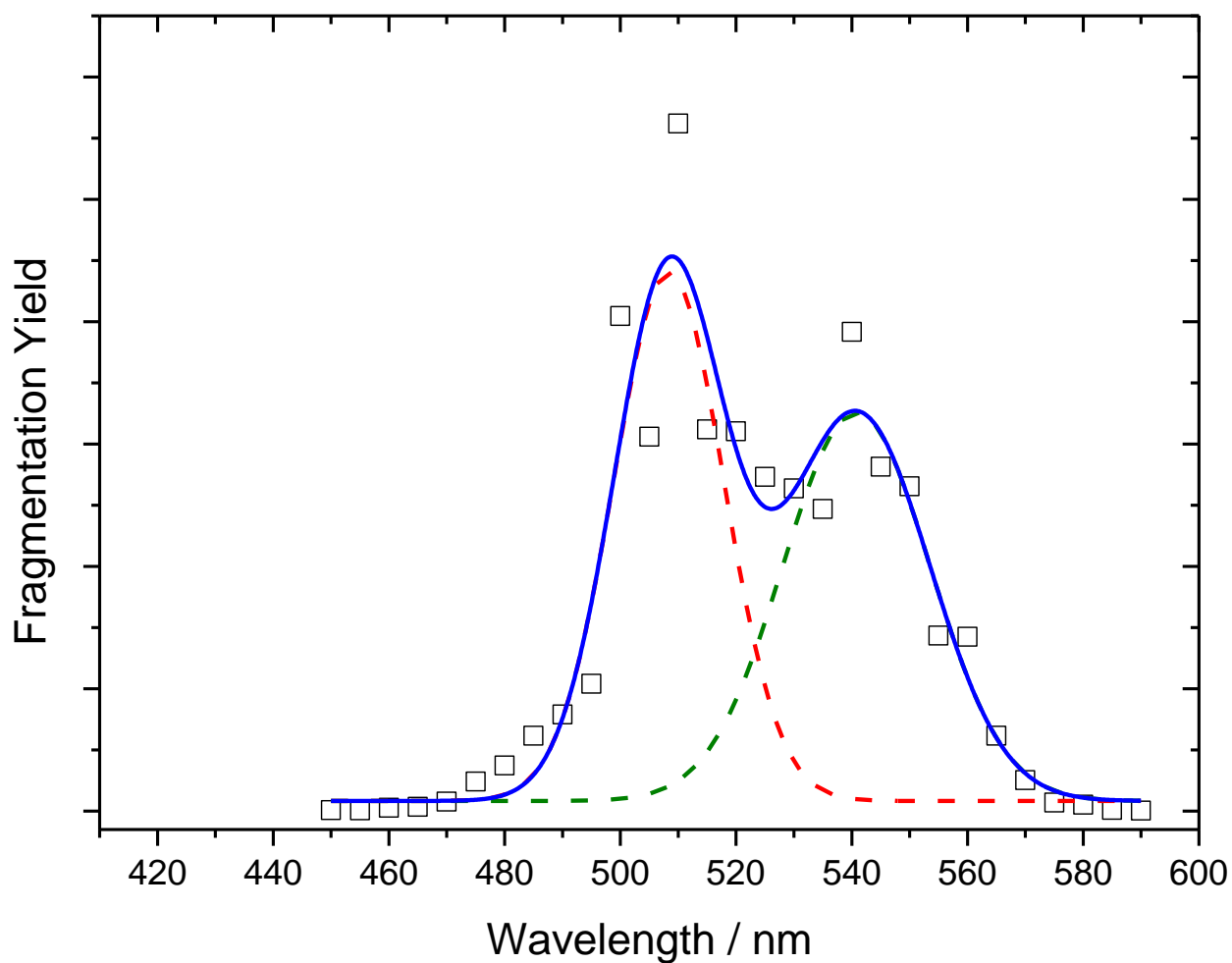


Figure S10. The fitted raw action spectrum of mass-selected $(\text{Rh575-KA}_2\text{HA}_2\text{K-QSY7})^{3+}$ (black squares). The dashed curves represent the fit to the QSY7 (green) and Rh575 (red) absorption bands. The solid blue curve represents the total fit.

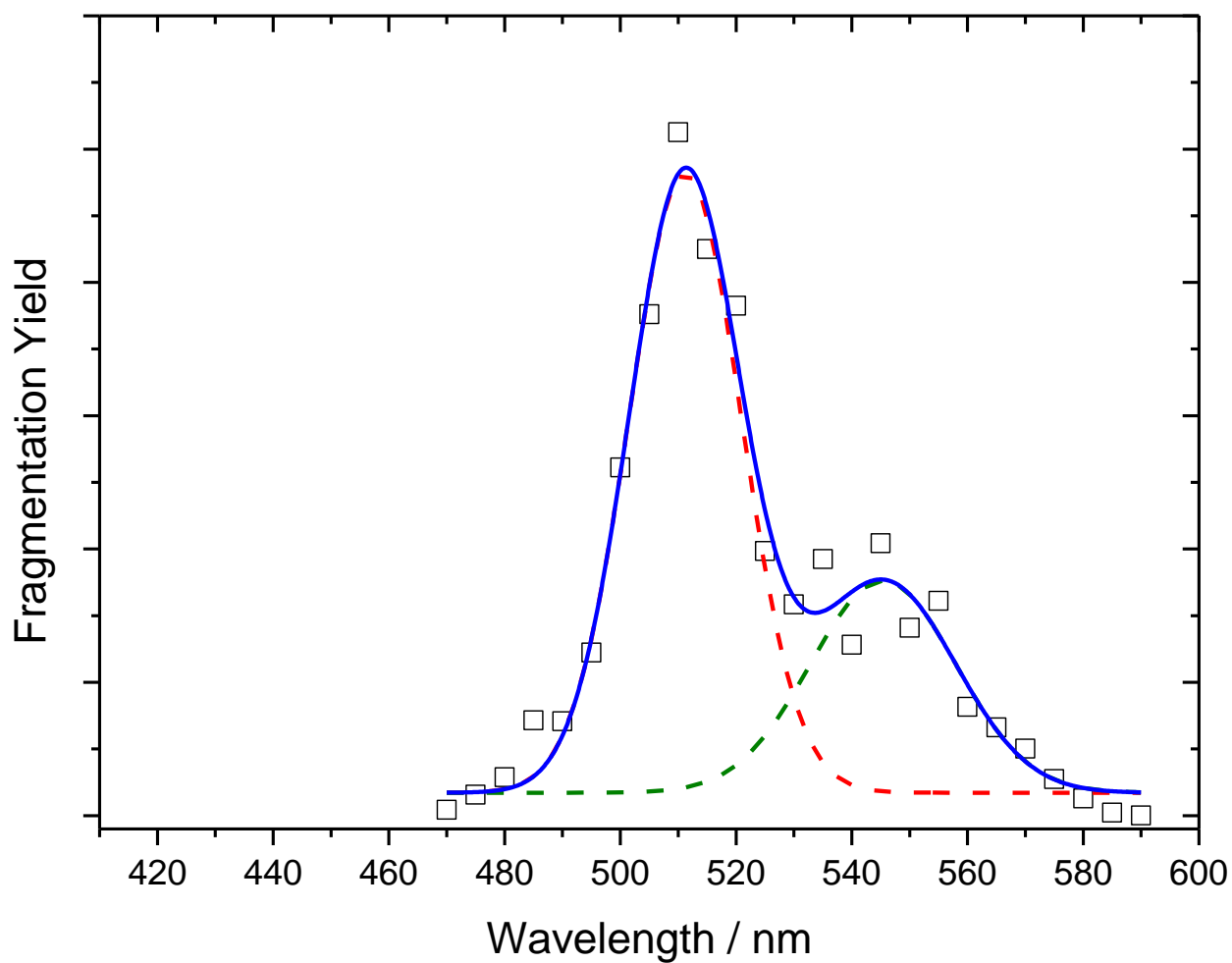


Figure S11. The fitted raw action spectrum of mass-selected $(\text{Rh575-KA}_5\text{HA}_5\text{K-QSY7})^{2+}$ (black squares). The dashed curves represent the fit to the QSY7 (green) and Rh575 (red) absorption bands. The solid blue curve represents the total fit.

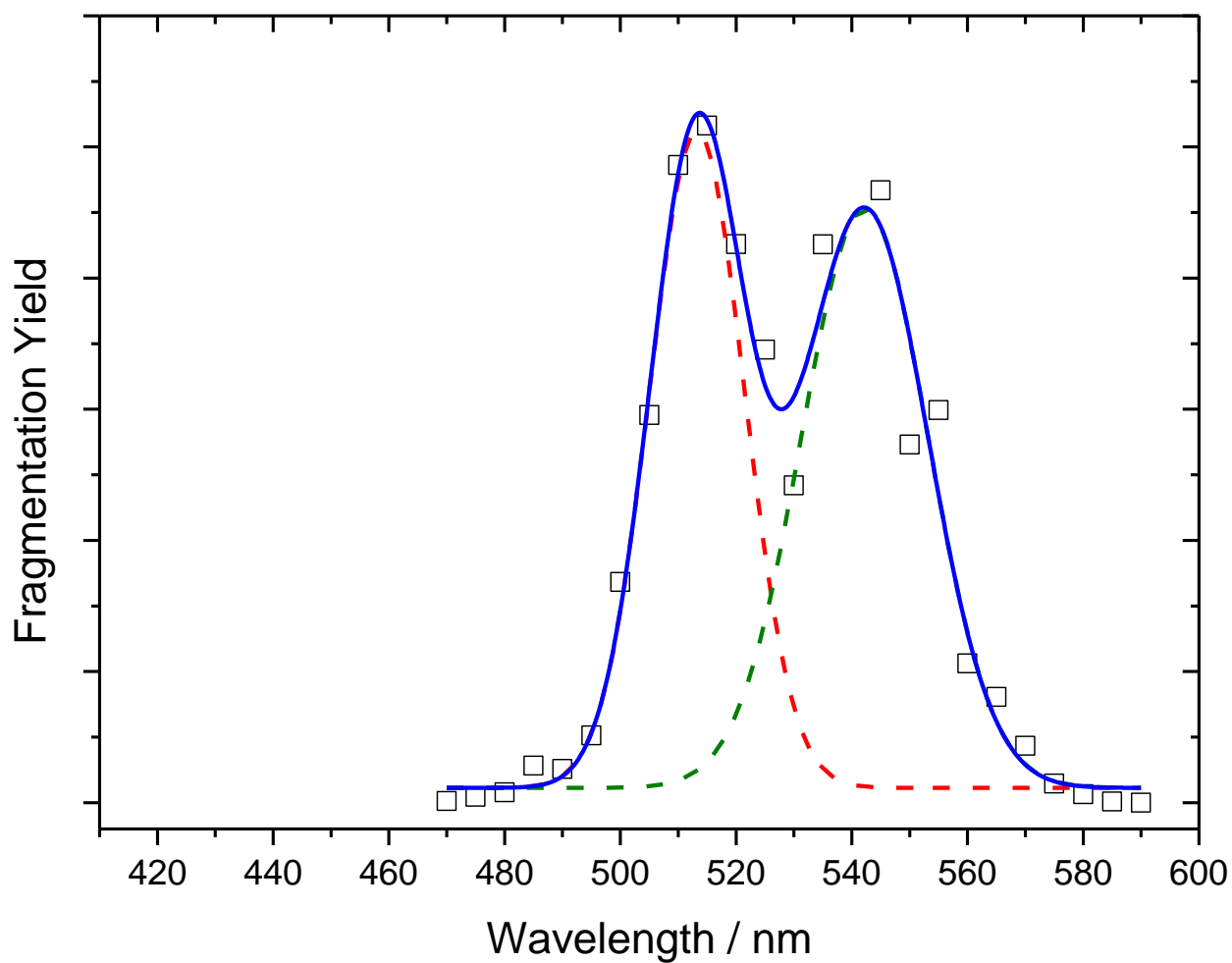


Figure S12. The fitted raw action spectrum of mass-selected $(\text{Rh575-KA}_5\text{HA}_5\text{K-QSY7})^{3+}$ (black squares). The dashed curves represent the fit to the QSY7 (green) and Rh575 (red) absorption bands. The solid blue curve represents the total fit.

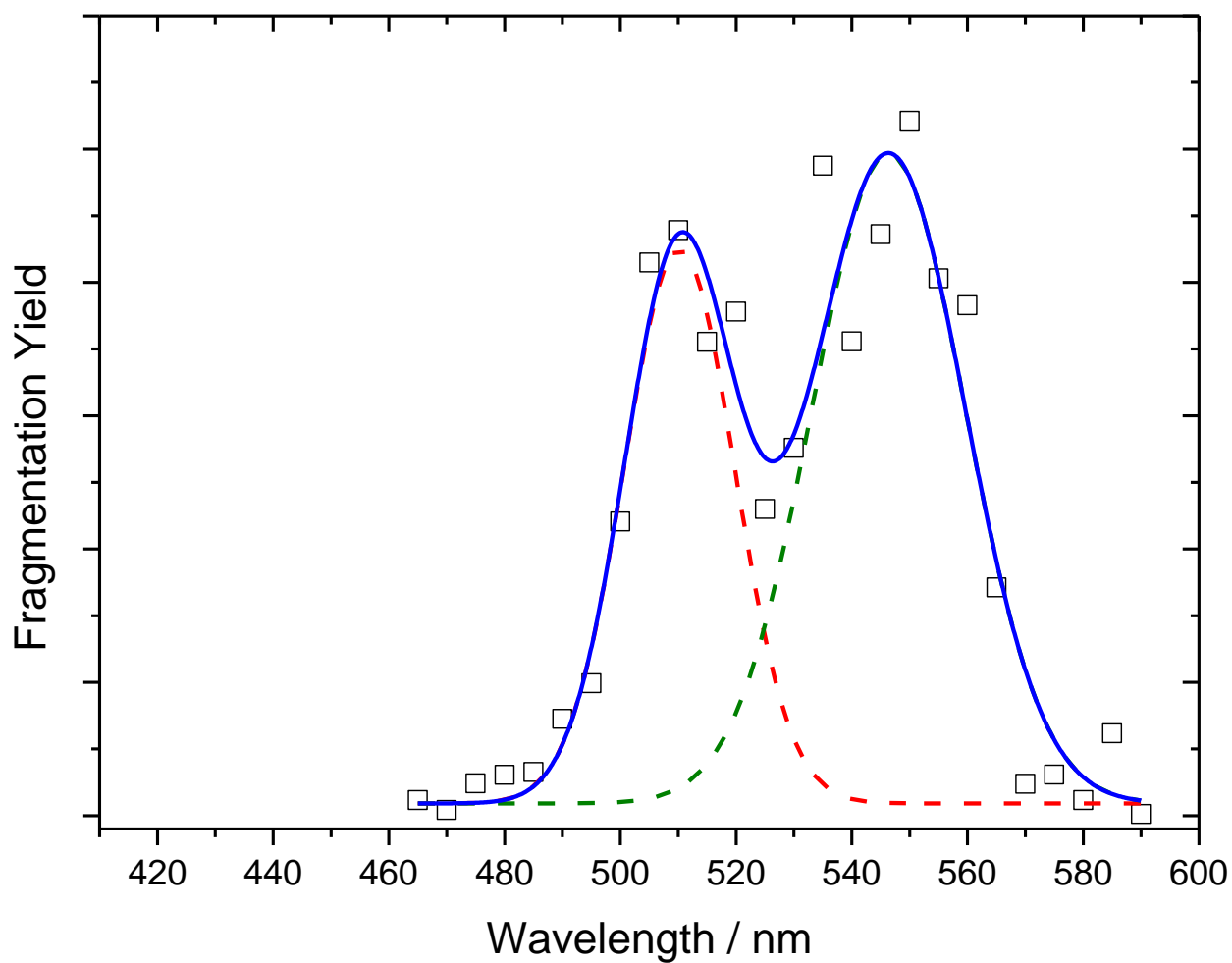


Figure S13. The fitted raw action spectrum of mass-selected $(\text{Rh575-KA}_5\text{HA}_5 \text{ HA}_5\text{K-QSY7})^{3+}$ (black squares). The dashed curves represent the fit to the QSY7 (green) and Rh575 (red) absorption bands. The solid blue curve represents the total fit.

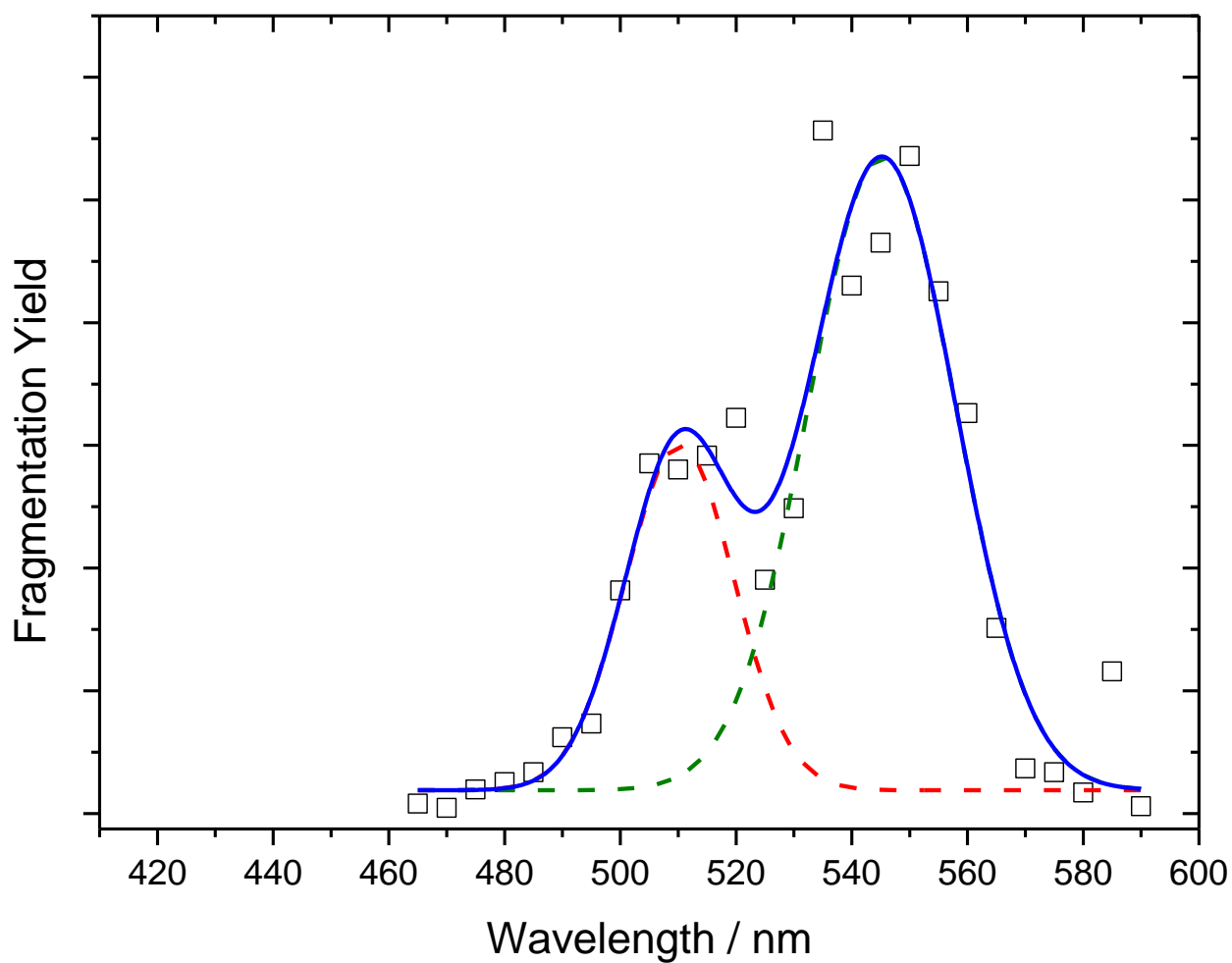


Figure S14. The fitted raw action spectrum of mass-selected $(\text{Rh575-KA}_5\text{HA}_5 \text{ HA}_5\text{K-QSY7})^{4+}$ (black squares). The dashed curves represent the fit to the QSY7 (green) and Rh575 (red) absorption bands. The solid blue curve represents the total fit.

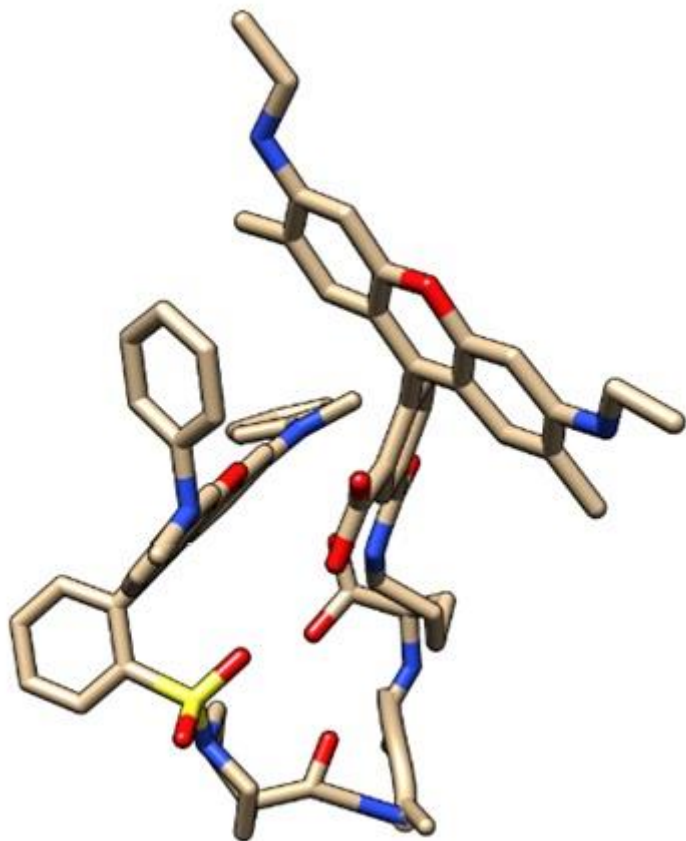


Figure S15. Lowest energy structure of (QSY7-AAK-rh575)²⁺ found by the Monte Carlo minimization program using the MMFF94 force field.